A NEW FIELD-DATA BASED EAF MODEL APPLIED TO
POWER QUALITY STUDIES

A THESIS SUBMITTED TO
THE GRADUATE SCHOOL OF NATURAL AND APPLIED SCIENCES
OF
MIDDLE EAST TECHNICAL UNIVERSITY

BY

MURAT GÖL

IN PARTIAL FULFILLMENT OF THE REQUIREMENTS
FOR
THE DEGREE OF MASTER OF SCIENCE
IN
ELECTRICAL AND ELECTRONICS ENGINEERING

SEPTEMBER 2009

Approval of the thesis:

A NEW FIELD-DAT BASED EAF MODEL APPLIED TO

POWER QUALITY STUDIES

submitted by **MURAT GÖL** in partial fulfillment of the requirements for the degree of **Master of Science in Electrical and Electronics Engineering Department, Middle East Technical University** by,

Prof. Dr. Canan ÖZGEN   _____
Dean, Graduate School of **Natural and Applied Sciences**

Prof. Dr. İsmet ERKMEN   _____
Head of Department, **Electrical and Electronics Engineering**

Prof. Dr. Muammer ERMİŞ
Supervisor, **Electrical and Electronics Engineering**   _____
Department, METU

Dr. Özgül SALOR
Co-supervisor, **TÜBİTAK-UZAY; Electrical and Electronics** _____
Engineering Department, Gazi Uni.

Examining Committee Members:

Prof. Dr. Aydın Ersak   _____
Electrical and Electronics Engineering, METU

Prof. Dr. Muammer Ermiş   _____
Electrical and Electronics Engineering, METU

Prof. Dr. M. Kemal Leblebicioğlu   _____
Electrical and Electronics Engineering, METU

Prof. Dr. Işık Çadırcı   _____
Electrical and Electronics Engineering, Hacettepe University

Dr. H. Bilge Mutluer   _____
TÜBİTAK-Uzay

Date: 10 / 09 /2009

I hereby declare that all information in this document has been obtained and presented in accordance with academic rules and ethical conduct. I also declare that, as required by these rules and conduct, I have fully cited and referenced all material and results that are not original to this work.

Name, Last name   : Murat GÖL

Signature   :

ABSTRACT

A NEW FIELD-DATA BASED EAF MODEL APPLIED TO
POWER QUALITY STUDIES

GÖL, Murat

M.SC., Department of Electrical and Electronics Engineering

Supervisor   : Prof. Dr. Muammer ERMİŞ

Co-Supervisor   : Inst. Dr. Özgül SALOR

September 2009, 73 pages

Electric Arc Furnace (EAF) modeling has been a common research area to date. This thesis work proposes a new field-data based EAF-specific model. The data used in developing the proposed model is obtained from field measurements of instantaneous voltages and currents of EAF the plants. This model presents the dynamic behavior of the EAF system including all its parts, which are the EAF transformer, the secondary circuit, the electrodes moving and the arc itself. It consists of a cascade connected variable-resistance and –inductance combination to represent the variation in time of the fundamental frequency, and a current source in parallel with it to inject the harmonics and interharmonics content of the EAF current. The proposed model is capable of representing both AC and DC EAFs, whose controllers' set points are the impedance values seen from the low voltage (LV) side of the EAF transformer. The validity of the proposed model has been verified by comparing EMTDC/PSCAD simulations of the model with the field measurements. The results obtained have shown quite satisfactory correlation between the behavior of the proposed model and

the actual EAF operation. To show the advantages of the model while developing FACTS solutions for power quality (PQ) problem mitigation of a given busbar supplying single- or multi-EAF installations, various applications are presented.

ÖZ

GÜÇ KALİTESİ ÇALIŞMALARINA UYGULANMIŞ
SAHA VERİLERİNE DAYALI YENİ BİR EAO MODELİ

GÖL, Murat

Yüksek Lisans, Elektrik-Elektronik Mühendisliği Bölümü

Tez Yöneticisi   : Prof. Dr. Muammer ERMİŞ

Ortak Tez Yöneticisi   : Öğr. Gör. Dr. Özgül SALOR

Eylül 2009, 73 sayfa

Elektrik Ark Ocağı (EAO) modellemesi yaygın bir araştırma alanı olarak günümüze kadar süregelmiştir. Bu tez çalışması saha verilerine dayalı yeni bir EAO'ya özgü model önermektedir. Önerilen modelin geliştirilmesinde kullanılan veriler EAO tesislerinin anlık akım ve gerilim değerlerinin saha ölçümlerinden elde edilmiştir. Bu model EAO sisteminin dinamik davranışını bütün elektriksel sistem parametrelerini kapsayarak (EAO transformatörü, sekonder devre, elektrot hareketleri ve ark) sunmaktadır. Geliştirilen model, temel frekanstaki değişimleri sergilemek üzere seri, değişken direnç ve reaktör kombinasyonundan ve EAO akımının harmonik ve ara harmoniklerini gösterebilmek için bunlara paralel bir akım kaynağından oluşmaktadır. Önerilen model, kontrol sisteminin ayar noktası EAO transformatörünün alçak gerilim tarafından görülen empedans değerleri olan AA ve DA EAO'ları ifade edebilmektedir. Modelin geçerliliği EMTDC/PSCAD programı kullanılarak yapılan benzetim çalışmaları ile saha ölçümleri karşılaştırılarak doğrulanmıştır. Önerilen sistem ve gerçek EAO operasyonunun karşılaştırılması ile

elde edilen sonuçlar, arada iyi bir korelasyon olduğunu göstermektedir. Modelin, tek ya da fazla sayıda EAO'yu besleyen belirli bir baradaki güç kalitesi problemlerine, esnek AA iletim sistemlerine dayalı çözümler üretirken sağladığı getirileri göstermek için çeşitli uygulamalar sunulmuştur.

Anahtar Kelimeler: Elektrik ark ocağı (EAO) modeli, saha verilerine dayalı model, güç kalitesi

To My Family

ACKNOWLEDGMENTS

I would love to express my deepest thanks and sincerest respects to my supervisor Prof. Dr. Muammer Ermiş for his guidance, advice, criticism, encouragements and insight throughout this research.

I would also love to thank my co-supervisor Inst. Dr. Özgül Salor for her mental support, assistance, suggestions and comments during my graduate studies. This work can hardly be possible without her effort and availability.

I acknowledge for the technical assistance of Prof. Dr. Işık Çadırcı gratefully.

I would love to express my appreciation to Mobile Power Quality Measurement Team of National Power Quality Project for sharing the data collected from various arc furnace plants. I also thank all TÜBİTAK-Uzay Power Electronics Group personnel for their helps throughout my research work and the research environment, which they provided.

I also express my thanks to my friends, who never left me alone whether they are near or far, for their trust, patience and support.

Finally and foremost, I thank my parents Süheyla and İbrahim, for their life-long guidance and unlimited support. I thank my sister, Başak for her trust in me. And special thanks go to my dearest fiancée, Ebru Aydın.

TABLE OF CONTENTS

LIST OF TABLES

TABLES

LIST OF FIGURES

FIGURES

CHAPTER 1

INTRODUCTION

An electric arc furnace (EAF), which heats charged material by means of an electric arc, is one of the principle furnace types for production of steel by electric power. The charged material is directly exposed to the electric arc and the current in the arc furnace electrodes passes through the material. EAFs range in size from small units of approximately one ton capacity up to about 400 tons and they are used for secondary steelmaking. EAFs are also used in research laboratories and by dentists with a capacity as small as a few dozen grams. Today, arc furnaces are widely used in steelmaking industry for their advantages as allowing steelmaking from a 100% scrap metal stock and reducing the energy required for steelmaking. On the other hand, highly varying excessive power demand of EAFs usually has adverse effect on the power quality of the electricity system supplying the EAF. Power quality is defined as the characteristics of the electricity at a given point on an electrical system, evaluated against a set of reference technical parameters by the International Electrotechnical Commission (IEC) [1]. These parameters include voltage amplitudes, voltage and current interharmonics, flicker and unbalance of the three-phase voltage values. Time-varying current demands of the EAFs usually cause harmonics, interharmonics and hence flicker and unbalance, which are most often tried to be avoided or reduced with the use of compensation systems to improve the quality of the power. Harmonics are the frequency components that are integer multiples of power system fundamental frequency, whereas interharmonics are the frequencies that are non-integer multiples of power system fundamental frequency [2]. Flicker is the impression of unsteadiness of visual sensation induced by a light stimulus whose luminance or spectral distribution fluctuates with time, while

unbalance is a condition in a poly-phase system in which the rms values of the line voltages (the fundamental component), or the phase angles between consecutive line voltages are not all equal [1]. Existence of harmonics, flicker and unbalance has adverse effect on the power quality (PQ) of the electricity system, which supplies the EAF plant.

This thesis focuses on developing an EAF model, which exploits actual field measurements taken at EAF plants, to be used for both compensation system design and for all kinds of analysis involving the electricity system supplying the EAF plant such as a new EAF installation at an existing plant. At this point, general information on EAF plant operation will be provided followed by the literature survey on EAF modeling and the scope of the thesis.

1.1   Electric Arc Furnace Operation Principles

EAFs are furnaces used to smelt scrap metal by means of electric arcs which can demand up to 240 MVA, and the temperature inside an EAF can rise up to 2000 degrees Celsius [4].

EAFs have some adverse environmental effects such as

- high electricity demand, followed by PQ problems,
- high sound levels,
- dust and off-gas production,
- slag production,
- cooling water demand.

Despite these harmful effects, EAFs are widely used in steel-iron industry, since they are highly efficient recyclers of the scrap material.

A typical EAF system is shown in Figure 1.1 from the Encyclopedia Britannica.

water-cooled panels
electrodes
electrode mast
steel melt
slag door
vertical taphole
ladle
refractory hearth
hydraulic rocker cylinder
cutaway view from front
exterior view from side
© 1999 Encyclopædia Britannica, Inc.
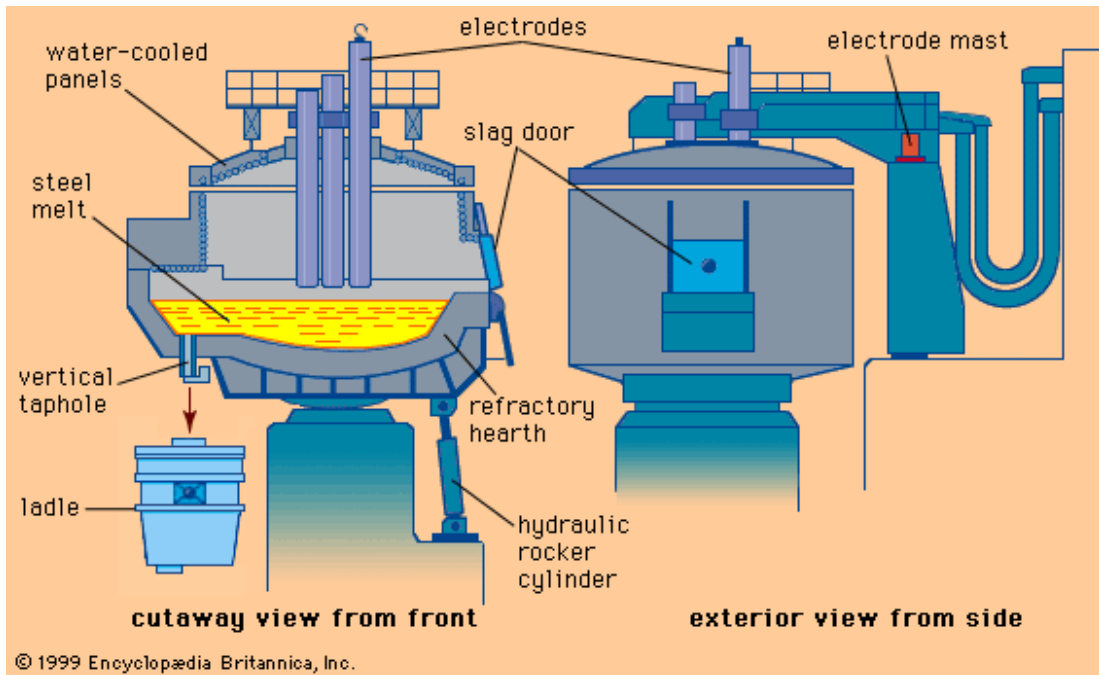
Figure 1.1   The EAF system.

An AC EAF has three round shaped electrodes corresponding to the three phases. The electrodes are automatically raised and lowered by either winch hoists or hydraulic cylinders controlled by a regulating system. The power system of an AC EAF is shown in Figure 1.2. It consists of the utility grid, a high voltage/medium voltage (HV/MV) power transformer, cables and/or O/H line segments, the EAF transformer, flexible cables, bus tubes and electrodes.
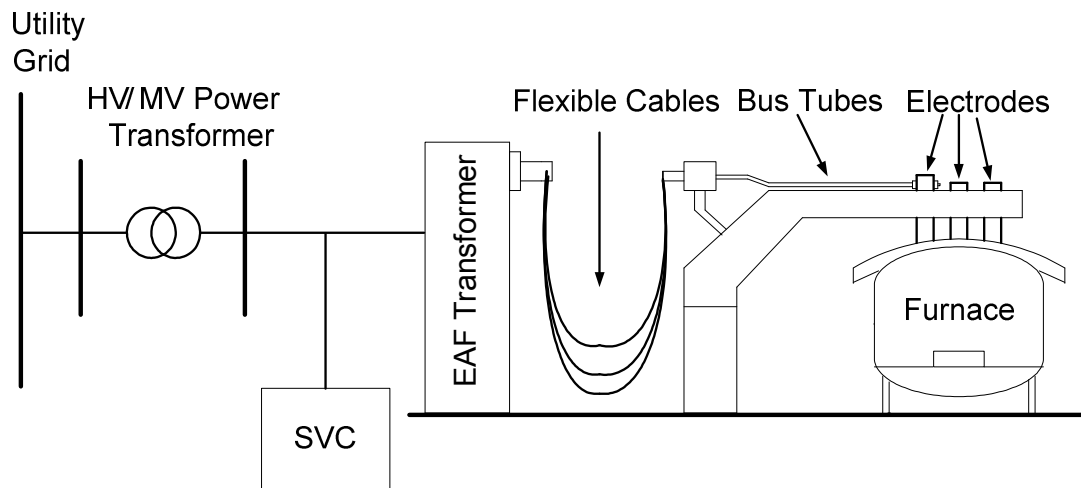
Figure 1.2   Illustration of the AC EAF power system.

A DC EAF has one round shaped electrode, conducting the DC current to smelt the scrap. DC current is achieved by rectifying the three phase AC current via a rectifier in front of the electrode. The electrode is automatically raised and lowered. The power system of a DC EAF consists of a rectifier and a DC link reactor different from an AC EAF system as shown in Figure 1.3.
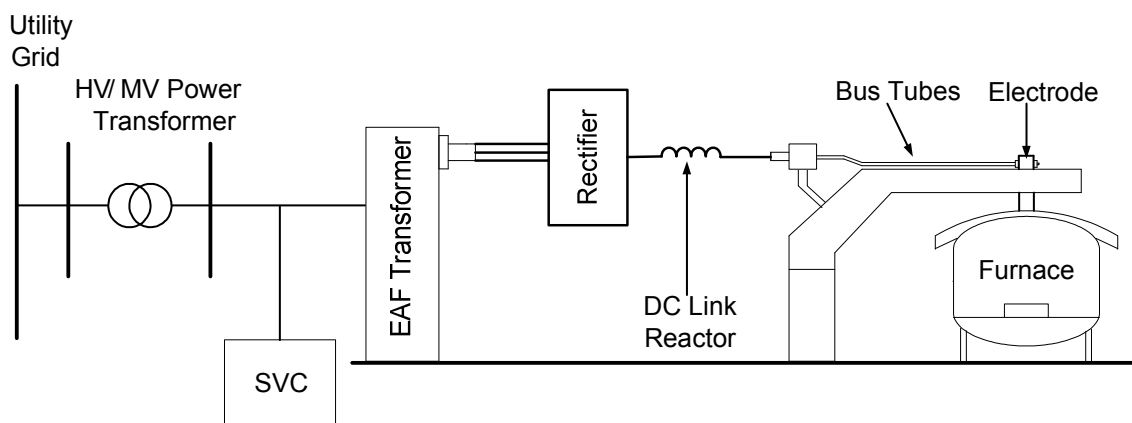
Figure 1.3   Illustration of the DC EAF power system.

The Static VAr Compensator (SVC) positioned between the EAF transformer and the power transformer, is an electrical device providing reactive power compensation and harmonic filtration.

The set-point for the regulation of the power system of an EAF is generally the impedance of the system to maintain the drawn current by the EAF constant and hence the active power spent. Not only are the positions of the electrodes but also the EAF transformer's taps changed in order to control the active power delivered. The taps are changed either by an operator manually or by a pre-programmed controller automatically.

The secondary circuit of the EAF is composed of flexible cables, bus tubes and electrodes as shown in Figure 1.2 and Figure 1.3. It constitutes nearly 75% of the total impedance as viewed from the low voltage (LV) terminals of the EAF transformer as illustrated in Figure 1.4 and varies in time during the operation of the EAF [5]. Furthermore, the non-linear arc resistance is changing dynamically depending not only on the state of the scrap and the molten material within the crucible but also on the electrode control system's settings and its capability to maintain the impedance at the set-point. Since the secondary circuit impedance and the arc resistance are referred to the primary side of the EAF transformer by the square of the turns-ratio, each tap changing causes a further variation. Therefore, the EAF is a highly inductive non-linear, unbalanced and rapidly changing load on the utility grid.
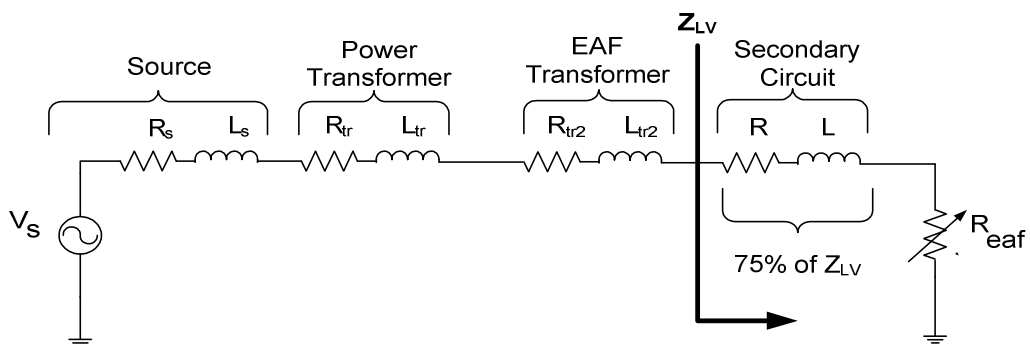
Figure 1.4   Illustration the EAF single-line diagram.

The smelting process of the EAF consists of three phases: Boring, melting, and refining [6]. The boring phase is the first part of the smelting process. In this phase the solid scrap metal is loaded into the furnace, and electric arc is initiated in the middle of the scrap to start smelting. The current reaches its most chaotic behavior and the most significant disturbance on the PQ is observed during this phase. When a hole in the middle of the scrap is achieved the electric arc becomes more stable, but due to the solid scrap that has not molten yet, the current characteristic is still unstable. This phase is called melting. The final phase, refining, is the most stable of all three, since whole material in the furnace is liquid so that arc length and hence the current demand do not vary as much as in boring or melting. The visualization of the three phases and the power variations during the three phases are given in Figure 1.5.
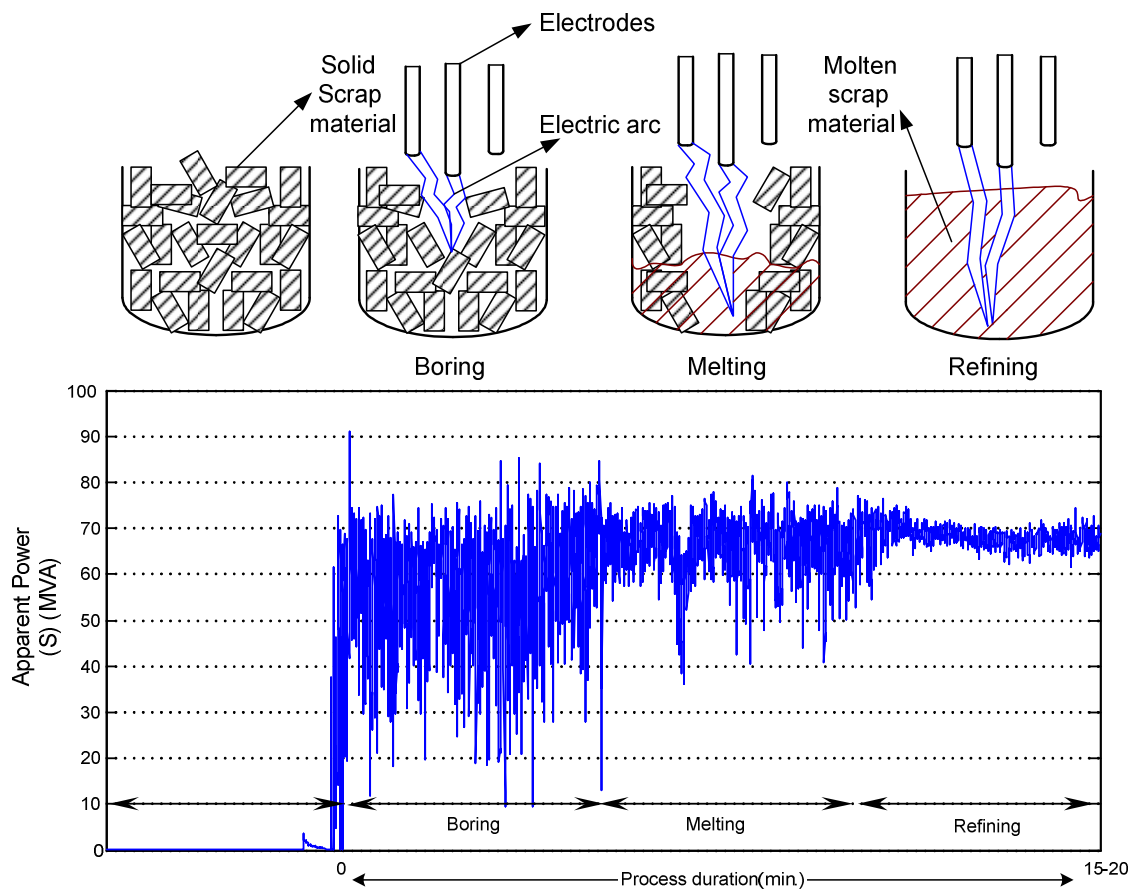
Figure 1.5   Illustration and power variation (one-cycle mean) of boring, melting and refining phases.

1.2   EAF Models in Literature

The EAF operation causes harmonics, interharmonics, flicker due to the strongly varying reactive power demand, therefore the PQ of the connected power grid is affected adversely. In order to study these undesirable disturbing effects, and possible compensation schemes in a simulation environment, developing a suitable model of the EAF operation has become a current issue and hence a popular research subject.

Developing a deterministic model of an EAF is not an easy task due to the stochastic nature of its operation. The current drawn by the EAF depends on the constituents and even the physical composition of the scrap to be smelted, which is random at each charge period. In addition, transformer tap adjustment applied by the operator and the impedances of the flexible cables supplying the EAF are subject to change due to the electrode movements during the EAF operation. Therefore, it is not easy to represent the EAF operation by a static model.

EAF modeling has been studied by many researchers to date [7-17]. The models in the literature may be classified in two groups as parametric models and field-data based models. Certainly some measurements have to be taken for both types. The measurements for the parametric model derivation are carried out to determine some parameters such as maximum magnitudes of harmonic and interharmonic components, extreme values of reactive power demand and other values necessary to identify the EAF. On the other hand, measurements, taken for field-data based model derivation, are used to determine the instantaneous characteristic of the EAF, such that the obtained result should match with the measured data, whereas in the previous type usually there is no such attempt.

Parametric models are based on the characteristic EAF operation [9-11]. These models are derived by using mathematical expressions. Deriving the mathematical expression of an EAF's exact characteristic is not an easy task, because it is not possible to obtain some of the EAF parameters. Therefore, generally some assumptions and simplifications are employed to obtain parametric models. This type

of models do not take into account the dynamic variation in the secondary circuits of the EAF and EAF-specific operational practices, but provide general aspects of the EAF operation instead. Therefore, it is rather difficult to use them for PQ assessment experiments on a specific plant.

Field-data based models may also be investigated in two subgroups; classical field-data based models and advanced field-data based models. Measured values are directly used as a voltage or a current source in classical field-data based models [12]. Although this type of a model provides the exact characteristics of a specific EAF, it cannot be used for PQ studies, since it does not take into account the voltage dependency of the EAF current and hence the effects of modifying power grid of the EAF in terms of PQ cannot be observed.

Advanced field-data based models use methods such as neural networks, fuzzy logic and chaos theory [13-17]. These models have obtained satisfactory results; however, the main drawback of these models is their complicated and time-consuming derivation process. These types of models derived so far represent only the furnace part of the EAF system. However, to simulate different situations, such as inclusion of a flexible alternating current transmission system (FACTS) device to the system, the model should be able to include the effects of the parts of the system other than the EAF itself. Also, the tap changing and electrode movements, performed to keep the current at a set value for constant power input to the EAF, are usually not considered.

1.3 Scope of the Study

In an iron and steel plant, the loads which are problematic in terms of PQ are EAFs, ladle furnaces (LFs) and rolling mills (RMs). EAFs are the dominant sources of harmonics, interharmonics, flicker and varying reactive power consumption, which are PQ disturbance factors, whereas LFs and RMs also cause comparably less significant PQ disturbances. Therefore, modeling the EAF operation is the main focus of this thesis. The aim of the thesis is to develop a field-data based EAF-specific model which can be used both to assess PQ and to develop solutions to

mitigate PQ problems in the simulation environment. The proposed EAF model represents the voltage dependent current characteristics of the EAF operation. Moreover, this model is capable of representing the effects of the tap changing process of the EAF transformer and also effects of the electrode movements.

The proposed EAF model is directly based on the measured field-data of instantaneous EAF voltages and currents sampled at a rate of 3200 samples per second. The operational impedance values of an EAF obtained from the current and voltage values at the primary side of the EAF transformer are used. Data are collected during the whole tap-to-tap period. Actually, as many data arrays as possible that can be collected are useful to consider not only different scrap compositions, but also different alloys recycled in the EAF. Analyses carried out with the proposed model have shown that simulation results coincide with the field-data collected from the associated EAFs at different plants. After the model is finalized, it has been used to obtain the effects of FACTS devices such as SVCs, static synchronous compensators (STATCOM), which are generally used for voltage regulation and reactive power compensation, and medium voltage active power filters (APF) usually employed for harmonic filtration on the PQ of the EAF installations.

The outline of the thesis is as follows: In Chapter 2, the proposed EAF model is described in detail including the alternative methods used to obtain the model, and their advantages and drawbacks. Finally, model usage is explained. In Chapter 3, the proposed model is verified by using various methods. The model is simulated in PSCAD/EMTDC for different circuit configurations, and the results are compared with the measured field-data, in the sense of harmonics, interharmonics, flicker, and active and reactive power produced and consumed by the EAF. In Chapter 4, some applications are performed in simulation environment. The model is simulated in a multi-furnace system. The obtained results are compared with the general expectations. Moreover, using the EAF model with SVC, STATCOM and APF are examined. Finally, in Chapter 5, conclusions are presented.

CHAPTER 2

THE PROPOSED EAF MODEL

2.1   The EAF Characteristics

The EAF current has a chaotic and random nature, which is the main reason of the PQ disturbing effects of the EAF. This current characteristic originates from the electric arc used to smelt the scrap material. Instantaneous values of virtual line-to-neutral voltage and line currents on the MV side of the EAF transformer excluding the SVC in Figure 2.1 are measured at a sampling rate of 3.2 kS/s (3200 samples per second) for each electrical quantity in all three phases. For line A these are plotted on v-i plane for one minute, one second and five cycle durations column wise in Figure 2.1. The three rows of Figure 2.1 correspond to boring, melting and refining phases. These plots show the stochastic characteristics of the EAF. During the operation of the EAF, the scrap material changes its state from solid to liquid and the air gap portions within the charge decrease. Electric arc becomes more stable as the molten metal content of the crucible increases. Therefore, the randomness in the v-i characteristics decreases due to this phenomenon as it can be understood from Figure 2.1.

The EAF power system can be represented electrically as shown in Figure 2.2. As mentioned in Chapter 1, current EAF models usually deal with modeling the arc resistance. This approach does not take the EAF transformer, the series reactor, if existing, and secondary circuit in the model, so that they are not sufficient enough to represent the whole system characteristics.
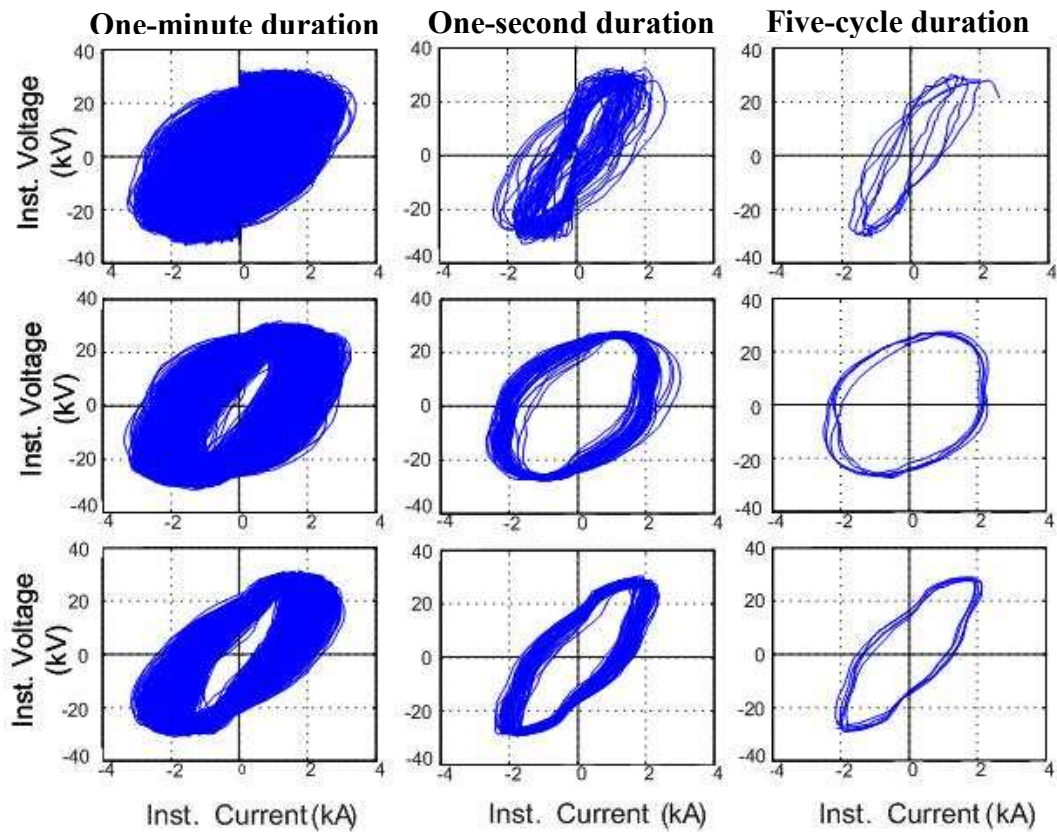
Figure 2.1　　Operational instantaneous v-i characteristic of a 90 MVA EAF
obtained from the field measurements (from transformer primary).
(Row 1: Boring, Row 2: Melting, Row 3: Refining)
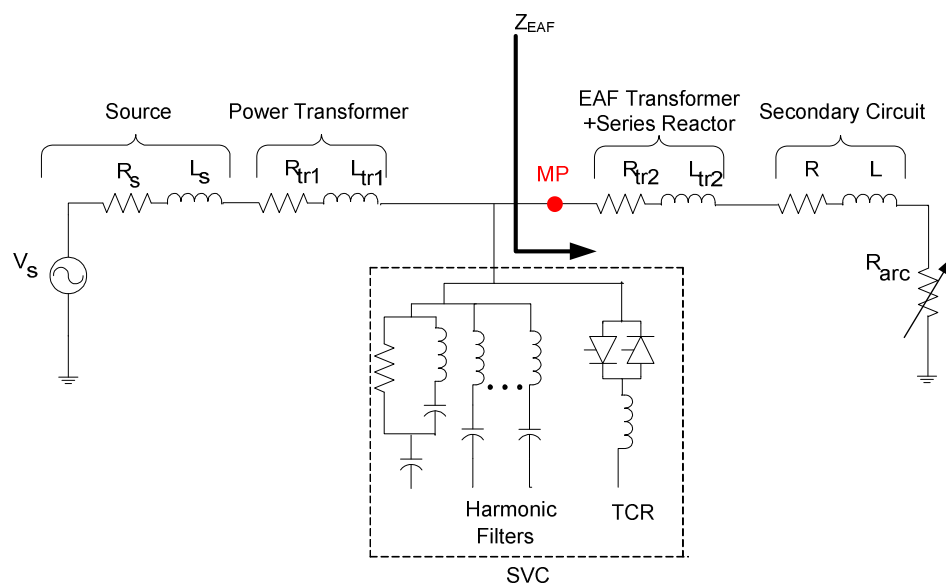
Figure 2.2　　EAF single-line diagram.

2.2 The Proposed Model of the EAF

The single-line diagram of the EAF on which the proposed EAF model is based is given in Figure 2.2. EAF is modeled as seen from the primary side of the EAF transformer as illustrated by Z_{EAF} in Figure 2.2 to represent the whole EAF system including the furnace, the secondary circuit, and the EAF transformer. The input-output relationship of the proposed EAF model based on the measured field-data of instantaneous three-phase EAF voltages and currents is given in Figure 2.3.

The proposed EAF model is developed by using measured field-data sampled at a rate of 3.2 kS/s. The model consists of the Variable-Resistance and -Inductance combination (VRL), and current harmonics denoted by $R[n]$, $L[n]$ and $I_H[n]$, respectively as given in Figure 2.3. This model can be used to predict the electrical quantities of the associated power system such as instantaneous voltages, currents, real and reactive power components, and short term and long term flicker values ($V[n]$, $I[n]$, $P[n]$, $Q[n]$, P_{ST} and P_{LT}, respectively).
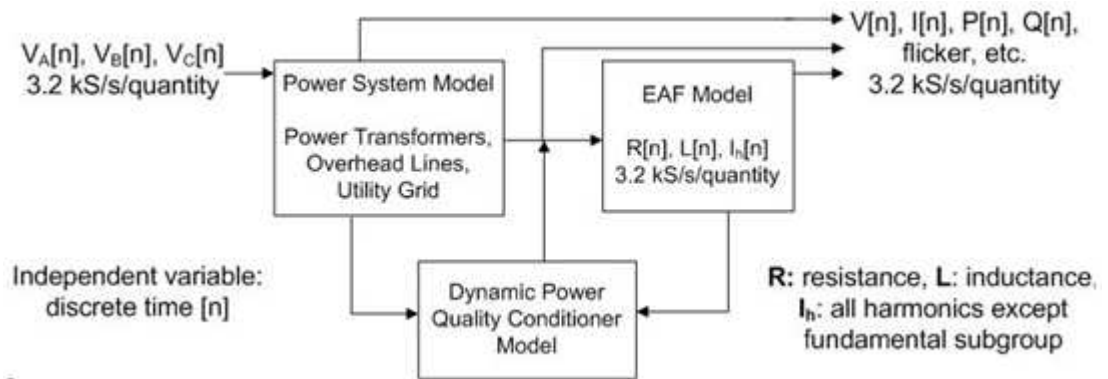
Figure 2.3   Input-output relationship of the proposed EAF system model.

The proposed model consists of the cascade connected VRL and a current source in parallel with the VRL as seen in Figure 2.4. By using the VRL, not only the time variations at the fundamental frequency (50/60 Hz) component are represented, but also the voltage dependency of the EAF current is taken into account. Equivalent

12

R-L combination as seen from the MV side of the EAF transformer computed from the field-data to constitute a VRL model is only for the fundamental frequency (50 Hz). The parallel connected current source injects the harmonics and interharmonics of the EAF current to the model.
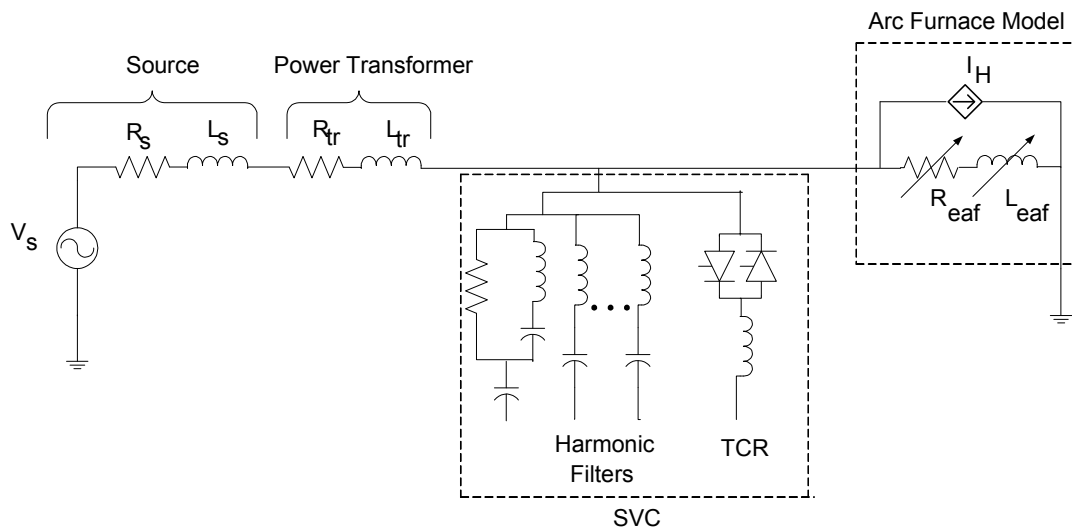
Figure 2.4   Single-line diagram of the proposed model.

Set points of the electrode control system are generally the impedance magnitude of the secondary circuit or the arc resistance value, since it is easy to measure and control the impedance magnitude by changing the arc length while moving the electrodes up and down. The impedance is determined by the electronic control system, using the phase voltage and the phase current data on the LV side of the EAF transformer [18]. Since the set point of the electrode controller is an impedance value, it is expected that the impedance value seen from the primary side of the EAF transformer oscillates around the set point for various conditions. Therefore, the impedance values obtained by processing the data measured are close for SVC-ON and SVC-OFF periods as seen in Figure 2.5. So the proposed model derived from the field-data can be used regardless of whether the data is taken when SVC is ON or it is OFF which eventually means that the proposed model is capable to provide the characteristics of the EAF system even there are devices connected parallel to it.

13
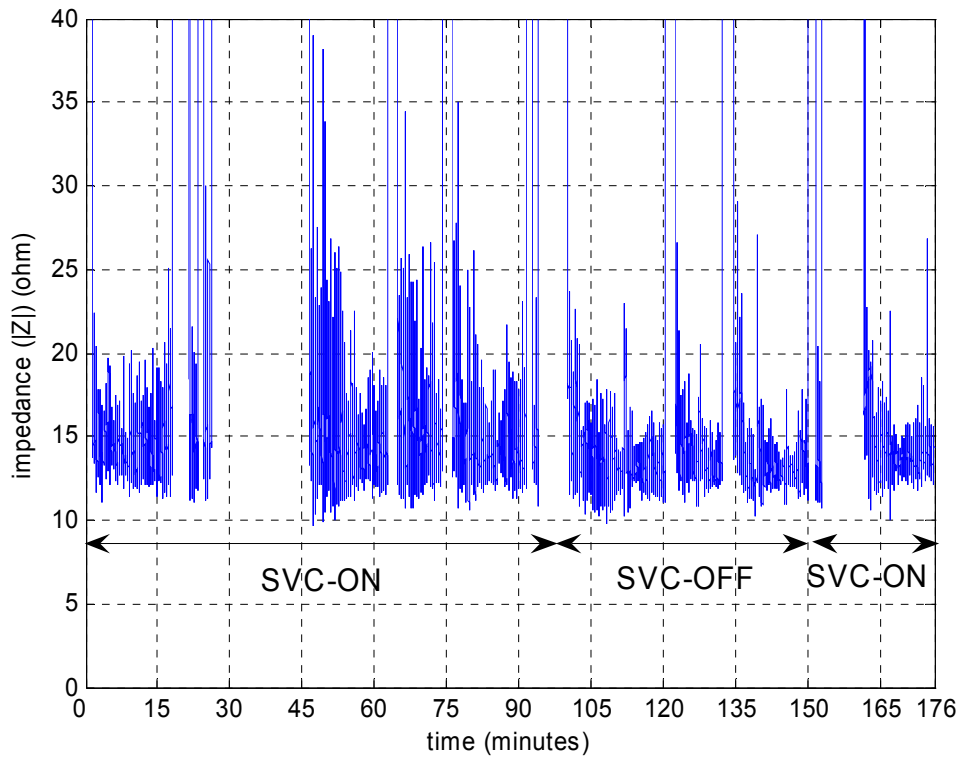
Figure 2.5   Impedance magnitude variations when the SVC is ON and OFF.

The block diagram of the VRL determination algorithm is given in Figure 2.6. It is a widely known fact that the power system frequency varies from 49.8 Hz to 50.2 Hz at the points close to EAF [19]. First, zero-cross points of voltage waveform are found on the measured data to determine the period of each voltage cycle. It is assumed that frequency of the current is the same with the frequency of the voltage. Zero-cross points of the voltage wave are used to determine 10-cycle windows for both voltage and current waveforms. Fast Fourier Transform (FFT) of each 10-cycle is obtained to achieve a 5-Hz-resolution frequency spectrum as recommended in the standard IEC-61000-4-7 [3]. Consecutive FFT windows are 10 cycles long and they are overlapping nine cycles, i.e. sliding by one cycle at each operation step. The windowing is illustrated in Figure 2.7. As observed in Figure 2.6 the absolute value of the 50 Hz component of the voltage divided by that of the current gives the absolute value of the impedance seen from the MV side of the EAF transformer. The difference between the phases of 50 Hz components of voltage and current gives the

14

phase of the impedance. The amplitude and phase values of the impedance are assigned to the mid-point of each sliding window; therefore, each cycle of the data is assigned an impedance value. Resistances and inductances are computed from the absolute value and the phase angle of the impedance. To obtain the inductance value, the frequency computed for every cycle after the zero-cross point detection is used as given in Figure 2.6. Finally, per-cycle VRL values are interpolated in order to obtain a VRL value for each time step (Δt_s=312.5μs). Example impedance values ($\mathbf{Z} = Z\angle\Phi$, magnitudes (Z) and phases (Φ)) obtained are plotted in Figure 2.8 for the boring, the melting and the refining phases. These impedances are computed from the field-data which was illustrated in Figure 2.1.
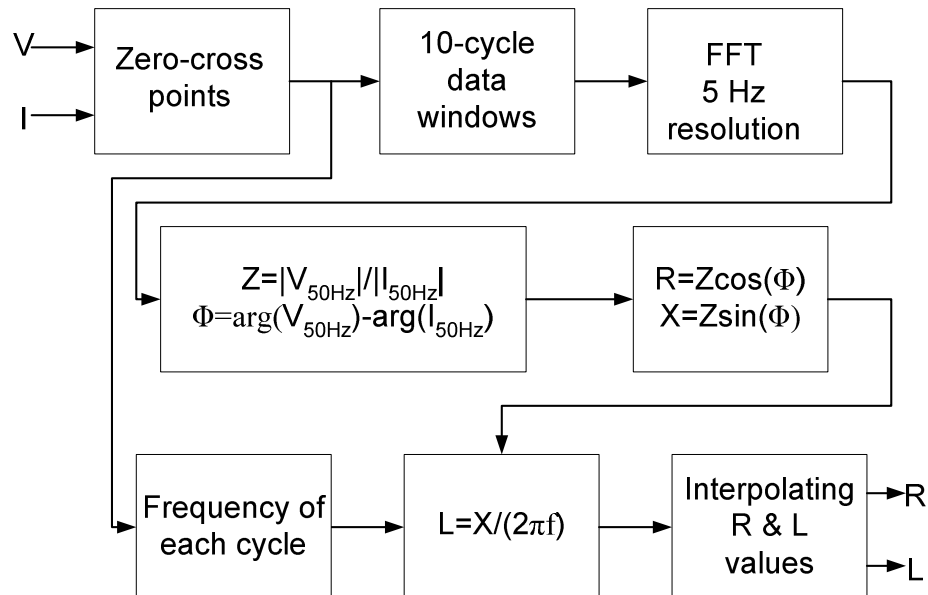
Figure 2.6   Block diagram of VRL determination.

15
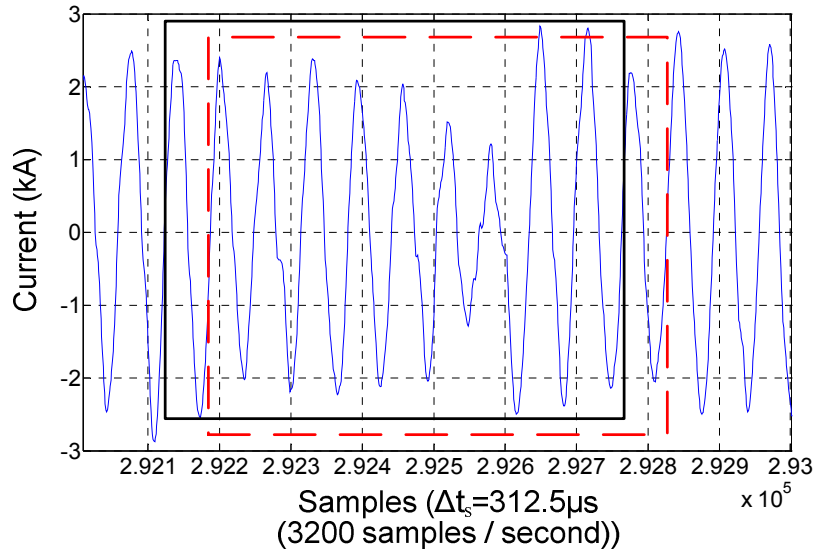
Figure 2.7   Windowing the actual current data (continuous lines represent the current window; dashed lines represent the window at the consecutive operation step).

One-minute duration   **One-second duration**   **Ten-cycle duration**

Sample (Δt_s=312.5µs)
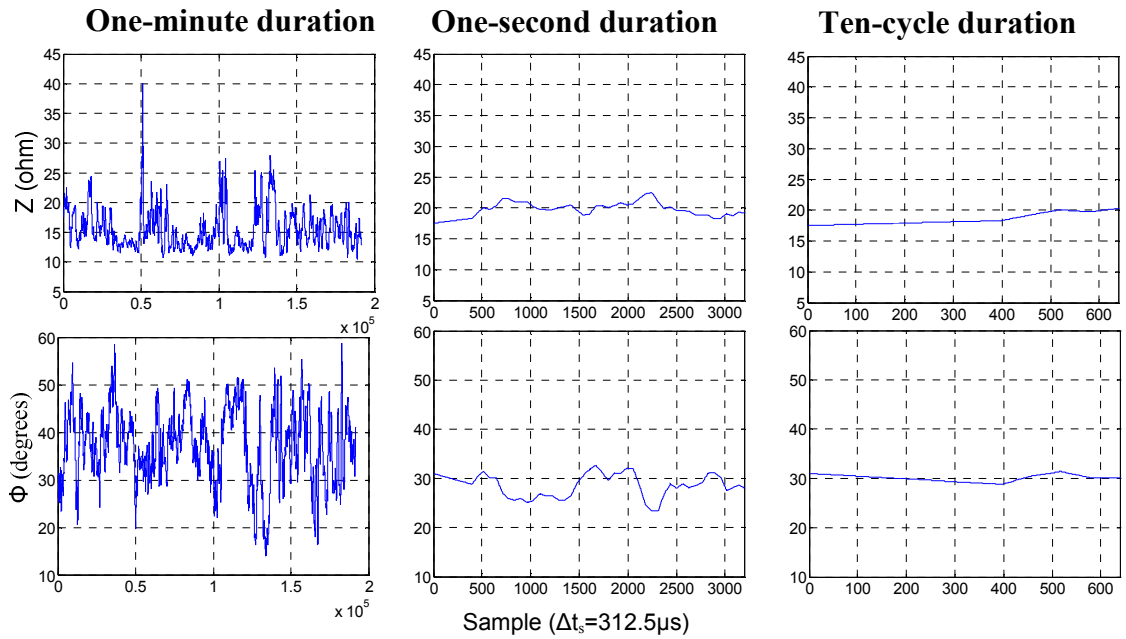
(a) Boring
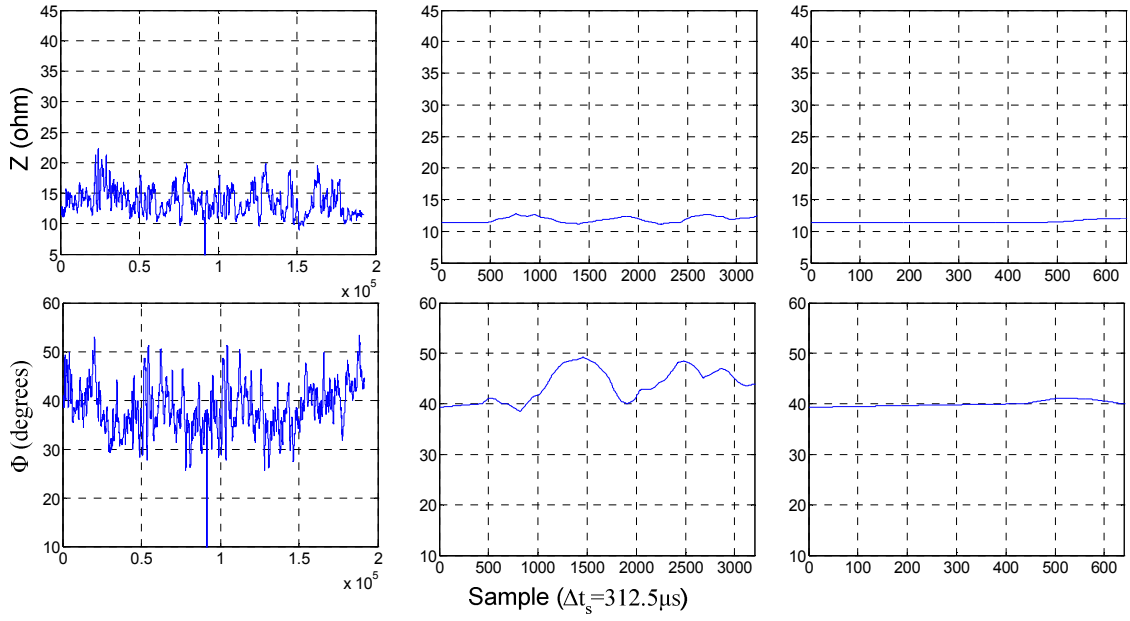
(b) Melting
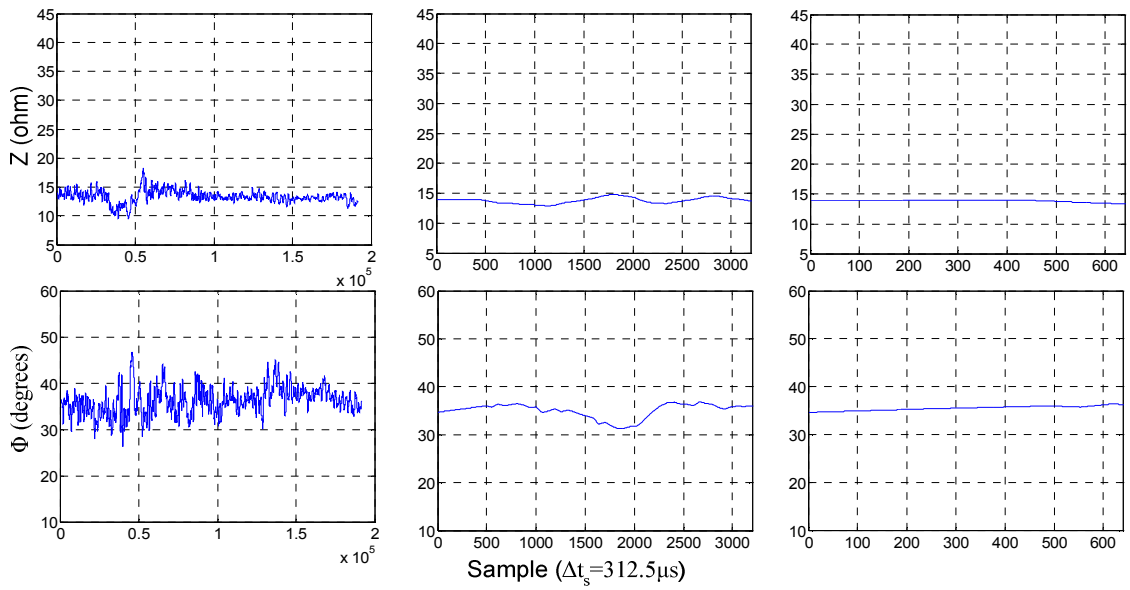
(c) Refining

Figure 2.8   Impedances and phases computed for each of the three phases.

Harmonic current is attained from the FFT of the original current for each 10-cycle window. The 50 Hz component of the current harmonic spectrum, which is the 10th component, is equaled to zero in order to eliminate the fundamental frequency, and hence 10-cycle-period average values of harmonic and interharmonic components are obtained. This spectrum is transferred back to time domain through inverse-FFT which represents the current supply of harmonics and interharmonics given in Figure 2.4 (I_H). This process is repeated for each cycle of the data to obtain the harmonic and the interharmonic current of one-cycle length. The 10-cycle windows slide one cycle at each computation step, as in the case of computing VRL values. Harmonic and interharmonic current computation is illustrated on example field-data in Figure 2.9. The block diagram of this process is shown in Figure 2.10. In Figure 2.9, it should be noticed that the signal obtained by taking the inverse-FFT of the reduced frequency spectrum of the current waveform is not a periodic signal, since there exist interharmonics with significant magnitudes in the spectrum of the current data measured.

I_H in Figure 2.10 includes all harmonics and interharmonics except fundamental frequency (47.5-52.5 Hz, due to the fact that the resolution is 5 Hz), and in the model in Figure 2.4, it is interpreted as a current source connected in parallel with the VRL. Controlled current source tool of PSCAD/EMTDC is employed for computer simulations of the proposed model.
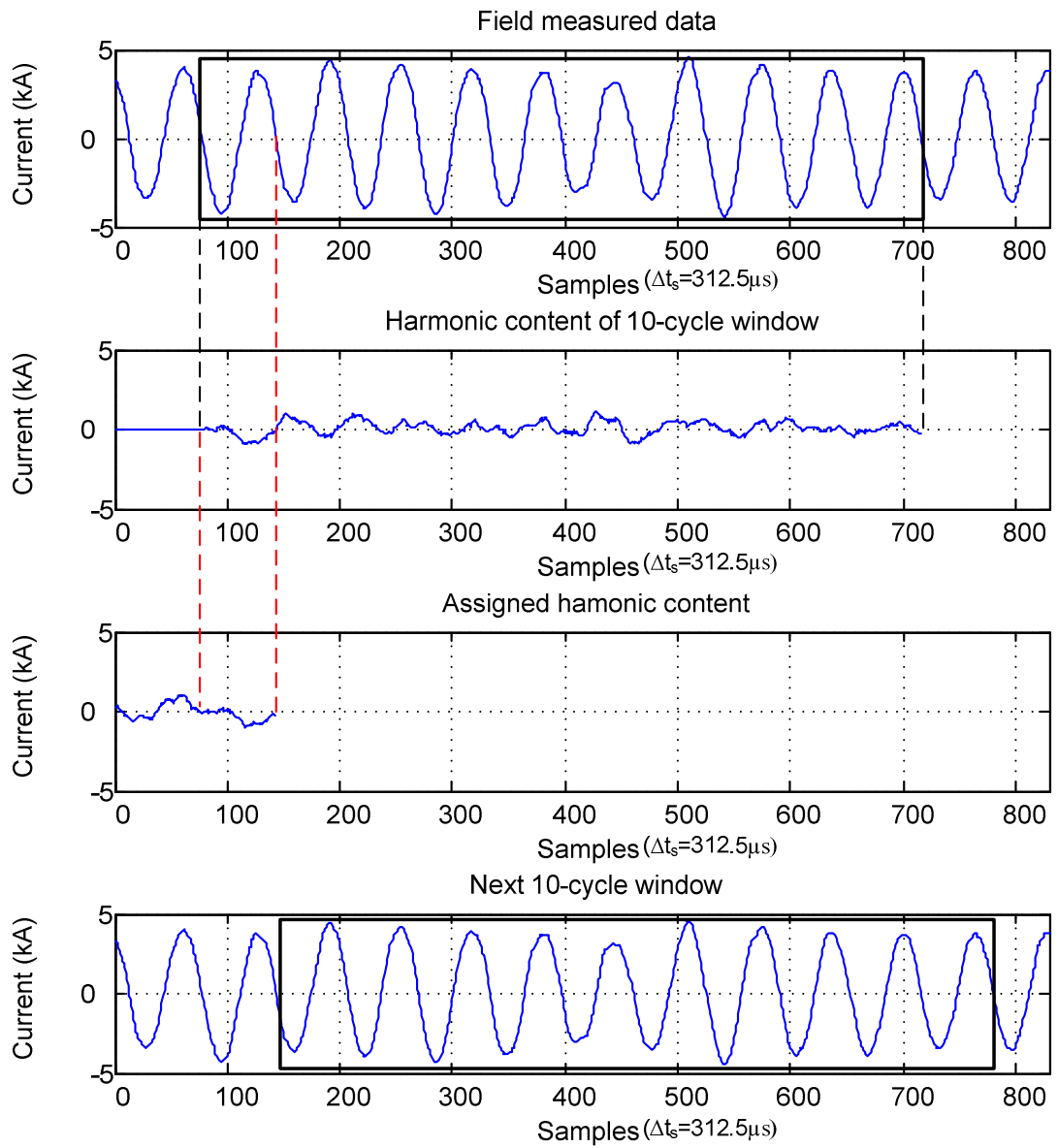
Figure 2.9   Harmonic current computation.
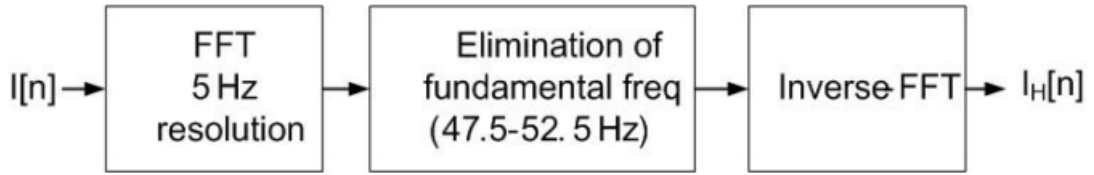
Figure 2.10   Block diagram of harmonic current computation.

2.3 Alternative Methods to Derive the Proposed Model

Although the results which will be presented in the following chapter show that the model works quite satisfactorily, alternative methods with less computational complexity but with less accuracy can be used to compute the VRL, and the harmonic and interharmonic components. These alternative methods are presented and compared with the proposed model in this subsection.

2.3.1 Alternative VRL Computation Methods

2.3.1.1   Method-1:

The exact frequency of the power system is calculated for each cycle in the proposed method, because actually the system frequency varies between 49.8 and 50.2 Hz [19]. The alternative method described in this subsection suggests assuming the system frequency constant at 50 Hz. Instead of calculating the zero-cross points of the field measured data, it is assumed that each cycle is 64 samples long for a sampling rate of 3.2 kS/s, and hence windows are 640 samples long. Comparison shows that although the order of the magnitudes and general characteristics of the currents are similar, there is a significant difference in sample by sample comparison as seen in Figure 2.11.
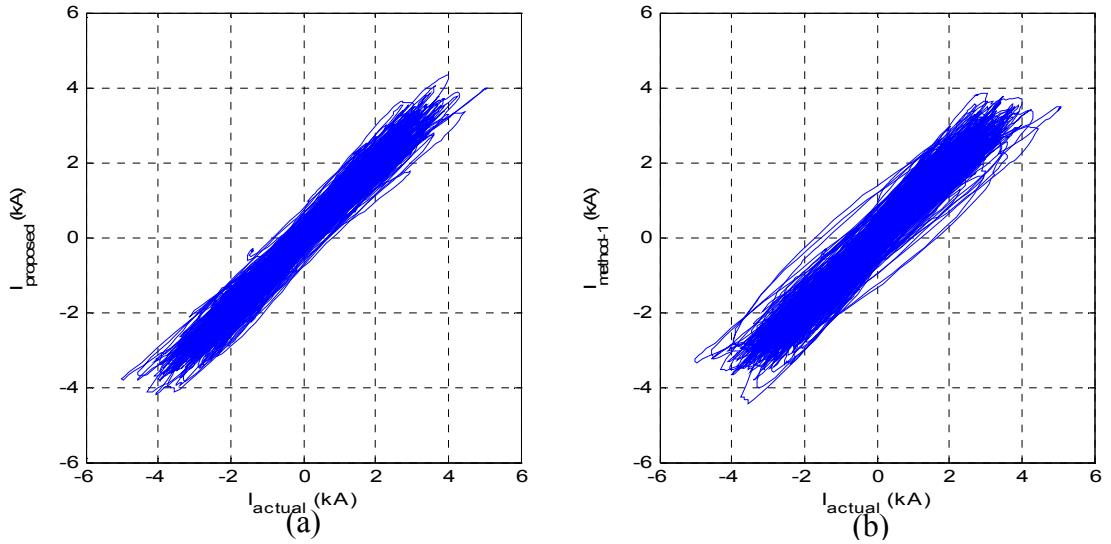
Figure 2.11   Instantaneous values of the EAF currents measured and computed at measurement point MP in Figure 2.1
a) $I_{proposed}$ vs. I_{actual} b) $I_{method-1}$ vs. I_{actual}.

2.3.1.2   Method-2:

The 10-cycle window used in the proposed algorithm slides one cycle for each computation step, which yields one VRL value for each cycle. To reduce the number of the computation steps, non-overlapping window of 10 cycles are used, which yield one VRL value for every 10 cycles of data. This reduces the computation by a factor of 10. Intermittent VRL values are obtained by linear interpolation. Figure 2.12 shows the comparison of the actual measured current and the results obtained by simulating the VRL achieved with this method. By comparing the results obtained in method-1 and method-2 (Figure 2.11 and Figure 2.12), it is concluded that, computing the actual frequencies at each cycle is more important to obtain a valid model than computing the impedance magnitudes for every cycle of the data.
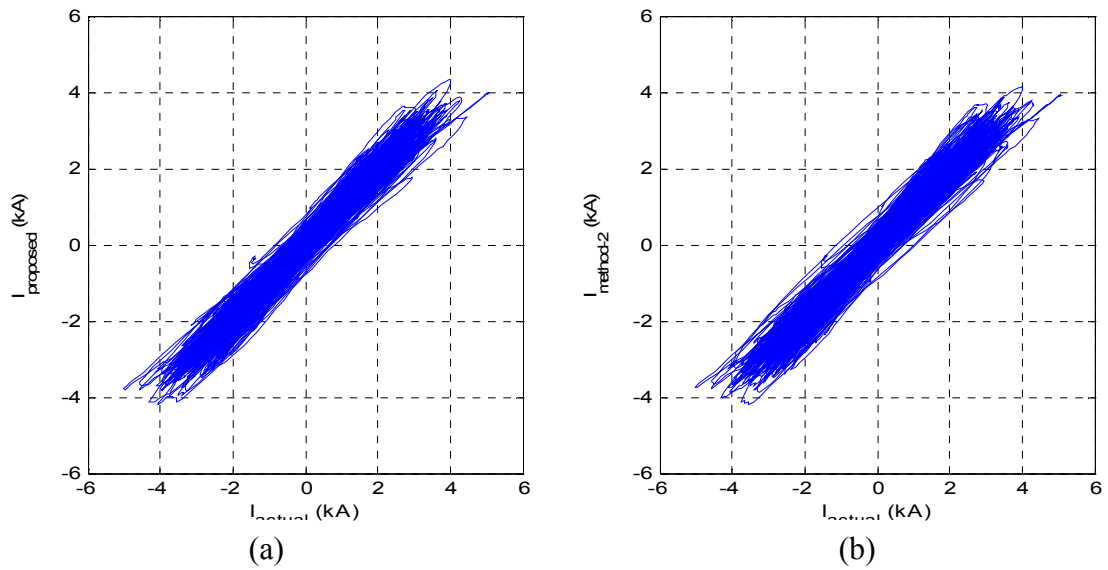
Figure 2.12   Instantaneous values of the EAF currents measured and computed at measurement point MP in Figure 2.1
a) $I_{proposed}$ vs. I_{actual} b) $I_{method-2}$ vs. I_{actual}.

2.3.2   Alternative Harmonic Current Computation Method

This method is based on the same idea as given in the previous subsection, "Method-2". Harmonic and interharmonic current computations are achieved using non-overlapping 10-cycle windows. Comparing the two methods does result in a significant difference as seen in Figure 2.13. When the 10-cycle window slides 10 cycles each computation step, the phases of the harmonic components becomes constant for whole 10-cycle period as well as the magnitudes; although, an average constant magnitude assumption does not result in a significant difference with the actual data, assuming the phases of the harmonic components constant whole 10-cycle period causes the difference seen in Figure 2.13.
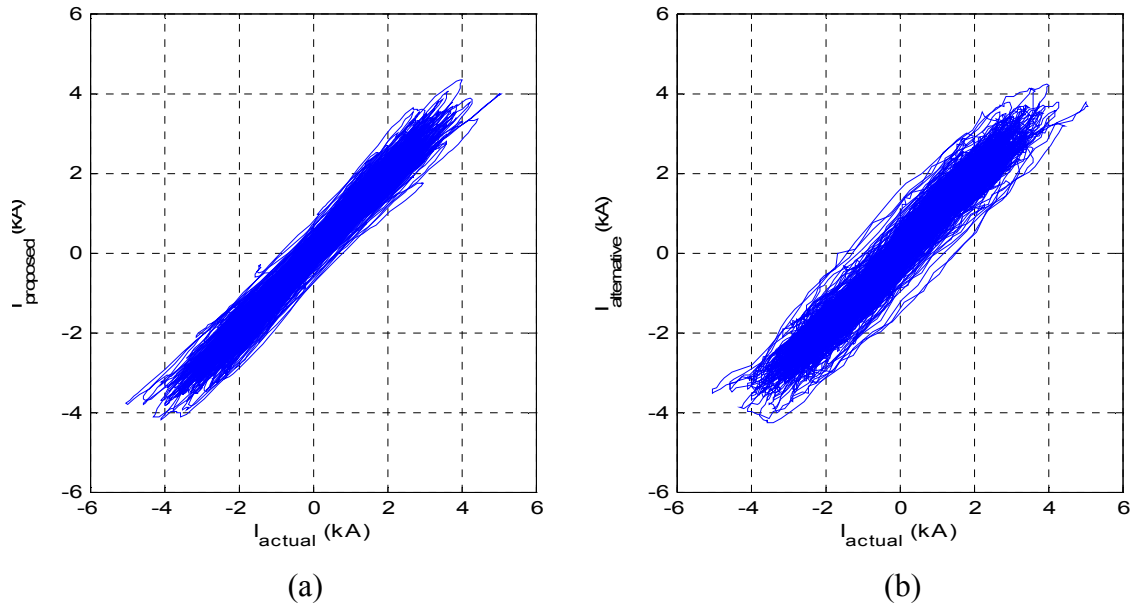
Figure 2.13   Instantaneous values of the EAF currents measured and computed at
measurement point MP in Figure 2.1
a) $I_{proposed}$ vs. I_{actual} b) $I_{alternative}$ vs. I_{actual}

2.4 How to Use the Model

The point of common coupling (PCC) is the point where EAF is connected to the
utility grid. The PCC is either the HV bus and EAF is connected through a power
transformer as given in Case-a in Figure 2.14, or it is the MV bus and EAF is
connected directly to the PCC as in Case-b. Source impedances can be computed
from the short circuit MVA values at HV and MV busses in Case-a and Case-b,
respectively in Figure 2.14. Case-a, however is the most common one.
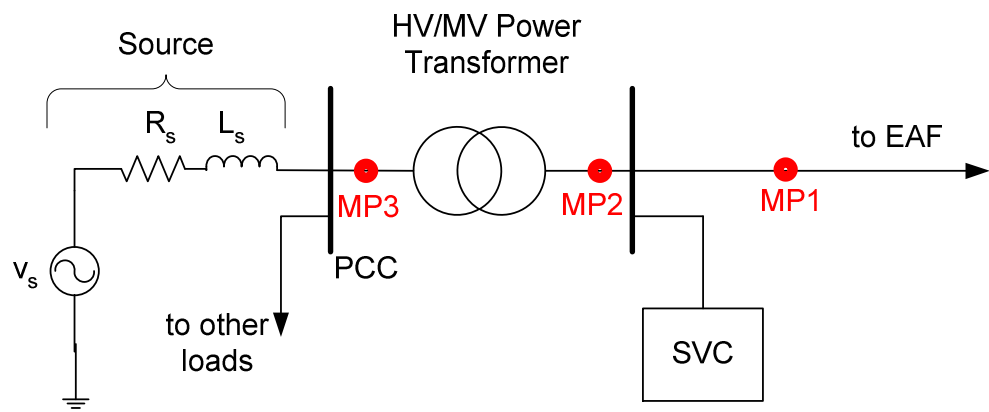
Case-a. HV bus is the PCC
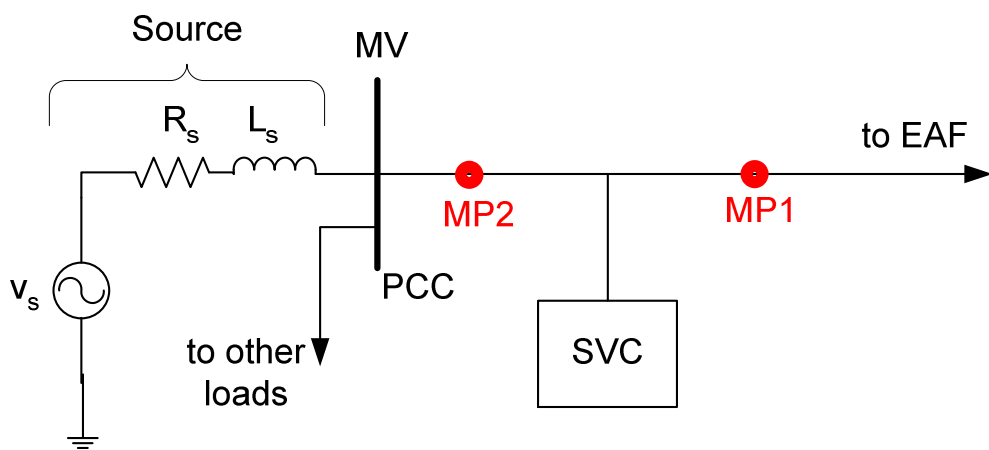
Case-b. MV bus is the PCC

Figure 2.14   Single-line diagram defining the Measurement Points (MPs) and Point of Common Coupling (PCC).

For application of the proposed method, time-synchronized measurements can be carried out at (Measurement points are shown by MPs in the figure)

i) MP1 and MP3 for Case-a,

ii) MP1 and MP2 for Case-b.

Bus voltages and line currents at each MP should be measured preferably at a high-sampling rate. The verification of the model needs the internal voltage of the utility grid (V_s in Figure 2.14) at any HV or MV bus to be known. V_s can be computed by using short circuit MVA (MVAsc) data and voltage and current measurement values at MP3 for Case-a and at MP2 for Case-b. Since V_s can be assumed to be balanced and purely sinusoidal at the fundamental frequency because of the low harmonic content of the voltage at PCC, its value can be found by phasor addition of the fundamental components of the three-phase voltages at MP3 and the potential drop on the source impedance owing to the fundamental components of the three line currents at MP3 for Case-a, and MP2 for Case-b.

This computation approach makes the expansion of the voltage and the current at MP3 into Fourier Series necessary in order to find their fundamental components, for Case-a. For Case-b purely sinusoidal internal grid voltages can be computed in a similar way.

Having computed the phases and magnitudes of the V_s, its time domain waveform is synthesized using EMTDC. This computation can also be achieved using any suitable computation software such as MATLAB. The EAF model is obtained from the measured current and voltage values at MP1 as explained previously in this chapter.

Although computation of V_s is a time consuming task, it is worth this effort since only by this way the variations in both the magnitude and the frequency of the utility grid voltage can be taken into account in the simulations and design work whenever accurate results are needed. If less accurate results are sufficient for the analyses of the quantities at the fundamental frequency such as P and Q variations, then V_s can

be assumed as an ideal voltage source without preserving its phase with respect to the measured EAF bus voltage.

Since the model is deduced from the field measurements at the input of the EAF transformer over typical tap-to-tap times, it exhibits the dynamic behavior of the EAF system including all parts of it such as the series reactor, the EAF transformer, the flexible cable, the bus tube, the electrode movements, and the arc.

CHAPTER 3

VERIFICATION OF THE MODEL

To validate the proposed model, measurements at five different EAF plants were conducted and the collected data are used for model verification. Measurement points (MP) for model verification are shown in Figure 3.1. VP is the virtual excitation point, where any measurement is not possible, but it is possible to compute voltages and currents at VP theoretically from measurements of voltages and currents at MP3, once the grid parameters, R_s and L_s, are known. R_s and L_s are calculated by using the MVAsc and rated voltage of the HV side of the power transformer. Verification of the model is achieved in five steps as given in the following subsections.
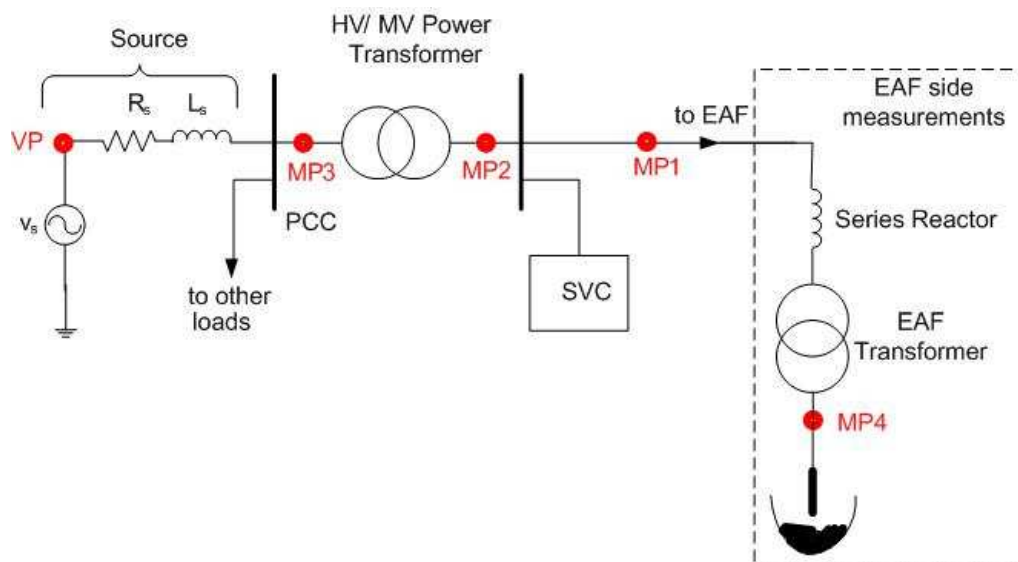
Figure 3.1   Measurement points shown on the single-line diagram for verification steps.

Field measurements are taken via monitors developed for PQ measurements through the National PQ Project of Turkey [20]. Time synchronization is achieved by a GPS module integrated into the PQ monitors. This gives the opportunity to collect data at MP1, MP2, and MP3 synchronously with only 100 nsec error among the collected data samples.

3.1   Step 1: Verification Based on the Measurements Obtained at the Secondary Side of the EAF Transformer (MP4)

Measurements for this step are taken at MP1 and MP4 synchronously for two tap-to-tap periods of the EAF transformer at Plant-1. The SVC was kept ON during one tap-to-tap period and OFF in the next. The aim here is to observe whether there exist significant differences between SVC-ON and -OFF periods of the EAF impedances due to the electrode control system of the EAF. It is worth noting that EAF transformer taps and the associated set values of the impedances are kept invariant for both SVC-ON and SVC-OFF periods.

In this step, actual EAF voltages and currents are measured in the field at the secondary side of the EAF transformer (MP4) and the results are compared with the same measurement carried out at the primary side (MP1) by taking into account the series reactor parameters, the leakage reactance and the turns ratio of the EAF transformer (see Appendix A for parameters of the EAF transformer in Plant-1 used in this step). The EAF impedances measured at MP4 using 10-cycle windows based on the fundamental EAF voltages and currents are given in Figure 3.2. EAF impedances are denoted by $|Z_{EAF,SEC}|=V_{f,SEC}/I_{f,SEC}$, where $|Z_{EAF,SEC}|$ is the impedance amplitude, $V_{f,SEC}$ is the amplitude of the fundamental component of the rms voltage, and $I_{f,SEC}$ is the amplitude of the fundamental component of the rms current, obtained from the secondary side of the EAF transformer.

In normal EAF operation, the impedance set-point is processed by filtering out the measured EAF currents and voltages to avoid high impedances except for ignition control. The impedances obtained at MP4 are median-filtered (of order 256 for a

28

sampling rate of 3.2 kS/s) to be able to observe the general behavior of the EAF excluding the instantaneous extreme points.
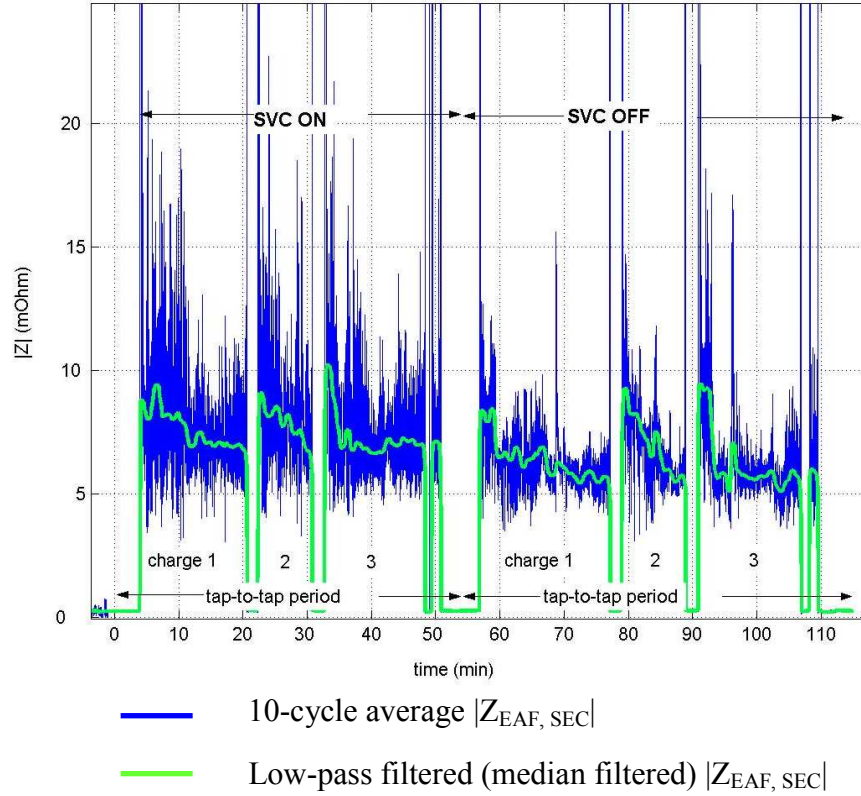
Figure 3.2   EAF impedance amplitude obtained from measurements at MP4 for two tap-to-tap periods with consecutive SVC-ON and –OFF periods.

During the EAF operation, the impedance set-point can be modified dynamically by the controller to allow an optimal usage of the EAF transformer taps. As seen in Figure 3.2, the actual EAF impedance for a tap-to-tap period does not vary considerably during SVC-ON and –OFF operations at the same EAF transformer tap. Hence, the proposed impedance model can be used satisfactorily for both cases.

In Figure 3.3, the EAF impedances are computed from true rms values of the EAF voltages and currents at MP4 by simple division ($|Z_{EAF,SEC}| \approx V_{SEC}/I_{SEC}$), and compared with the impedances obtained from the fundamental values as used in the

proposed model. The results obtained from two types of computations are almost the same, thus verifying the validity of impedance computation of the model.

$|Z_{EAF, SEC}| \approx V_{SEC}/I_{SEC}$ (true rms values)

$|Z_{EAF, SEC}| = V_{f,SEC}/I_{f,SEC}$ (fundamental values)
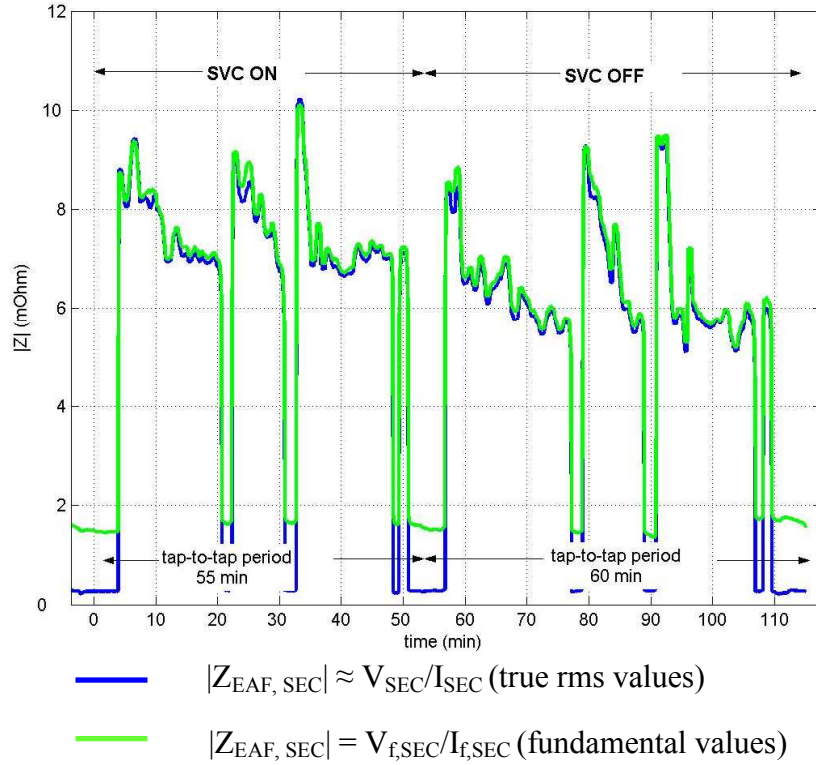
Figure 3.3   Low-pass filtered $|Z_{EAF, SEC}|$ at MP4.

Carrying out measurements at MP4 is found to be less practical than at MP1 due to the technical reasons and operational safety requirements of the EAF plant. Furthermore, the variations of the transformer and/or reactor taps cannot be represented directly by using measurements at MP4. It is, therefore, more convenient to base the proposed model on field measurements taken at the primary side of the EAF transformer (MP1) including the variations of the reactor and the transformer taps in the VRL part of the model, provided that the primary side measurements and secondary side measurements referred to the primary side correlate closely. Figure 3.4 proves this correlation. The discrepancy in high impedance portion of primary side measurements in Figure 3.4 belongs to the no-operation regions of the

EAF (open circuit condition). The primary of the EAF transformer remains energized between two charges whereas the secondary side is open (the electrodes are moved up).
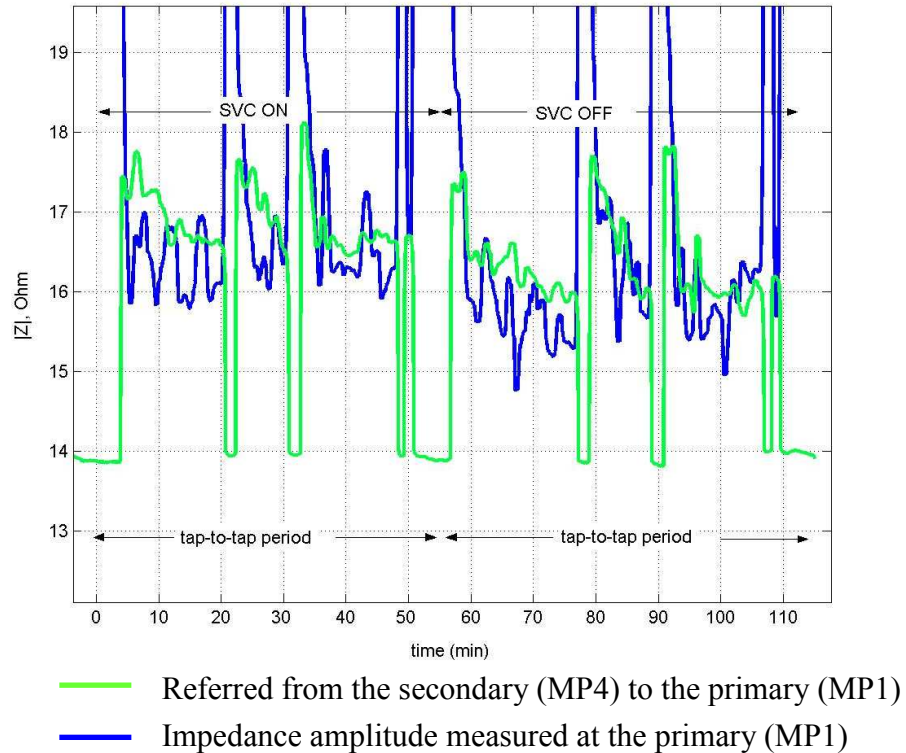
Figure 3.4   EAF impedance amplitudes obtained from MP1 directly and referred from MP4 to MP1.

3.2   Step 2: Verification of the EAF Model (VRL and I_H) Excited at MP1

In this step, measurements taken at Plant-2 are used. Voltage data collected at MP1 in Figure 3.1 is applied to the EAF model itself (VRL and I_H, the harmonic current source given in Figure 2.4) and the EAF current obtained is compared to the measured EAF current at MP1. To illustrate the comparison, 12 cycles of the obtained and the measured EAF currents for the boring, the melting and the refining phases of smelting are drawn in Figure 3.5. The actual EAF current and the one obtained from the model are plotted together in Figure 3.5. It is observed that both currents are nearly the same in both phase and magnitude.

31
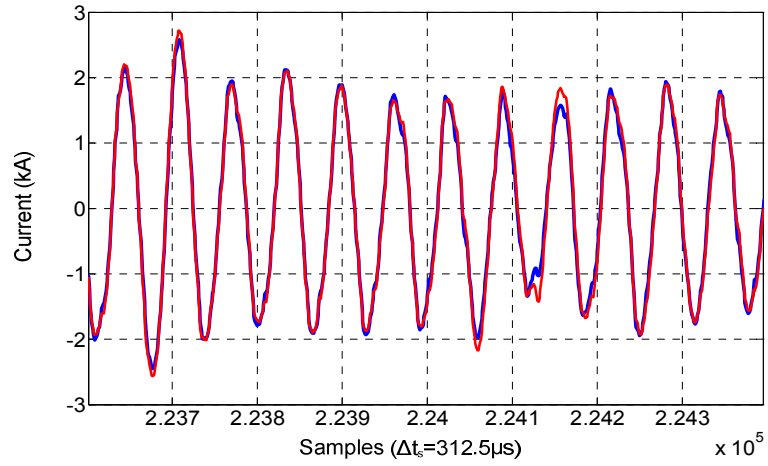
(a) Boring
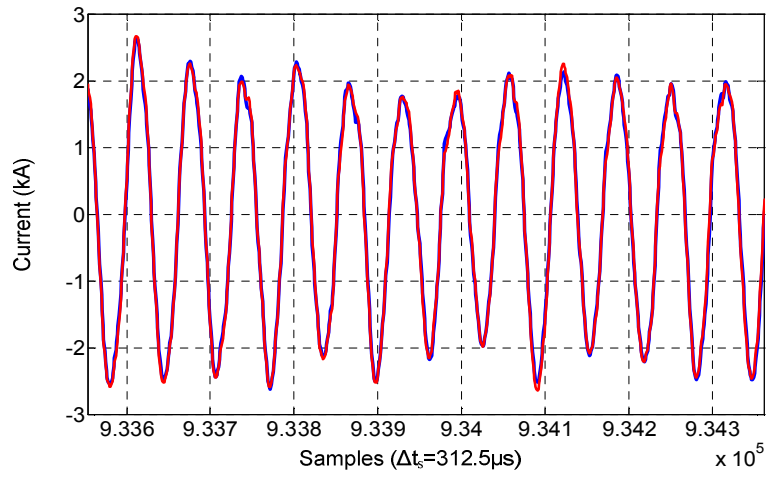
(b) Melting
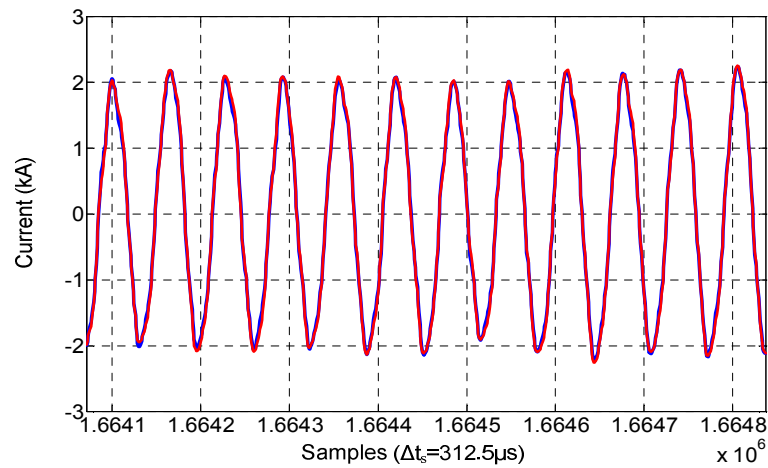
(c) Refining

Figure 3.5   The actual current at MP1 in Figure 3.1 and the simulation results obtained using the proposed EAF model plotted together.

Furthermore, the instantaneous current obtained from the model (I_{sim}) versus the actual instantaneous EAF current (I_{actual}) is plotted for a duration of nine minutes in Figure 3.6. It is observed that the actual and the model current samples are highly correlated. Frequency spectra are also compared in Figure 3.7. It can be seen from Figure 3.7 that harmonic and interharmonic compositions are almost the same. This verification step shows how closely the proposed model in Figure 2.4 corresponds to the actual EAF data collected at MP1.
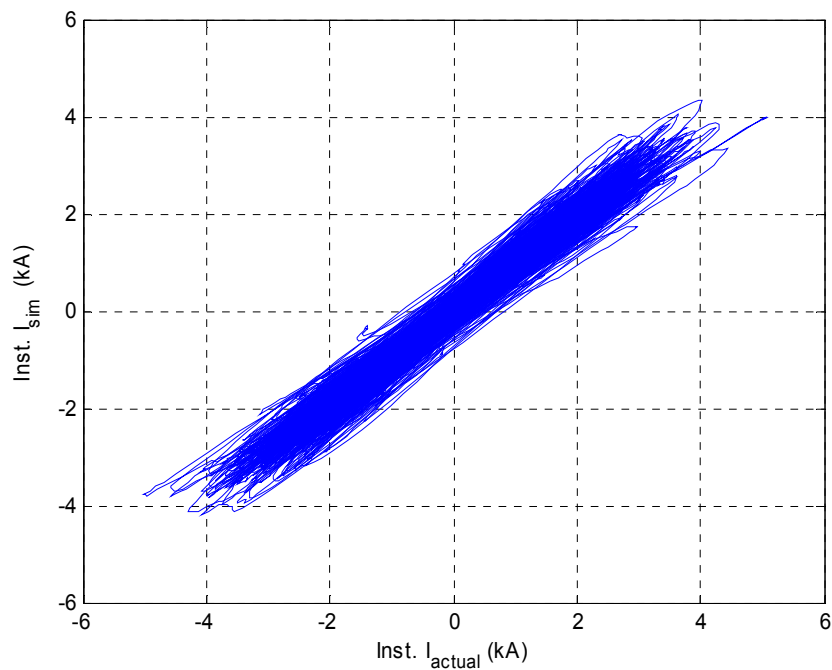
Figure 3.6 I_{sim} vs. I_{actual} (Instantaneous values).

(a) Frequency spectrum of the current passing through the VRL

(b) Frequency spectrum of I_H

(c) Frequency spectrum of the load current of the model, (a)+(b)

(d) Frequency spectrum of the actual load current
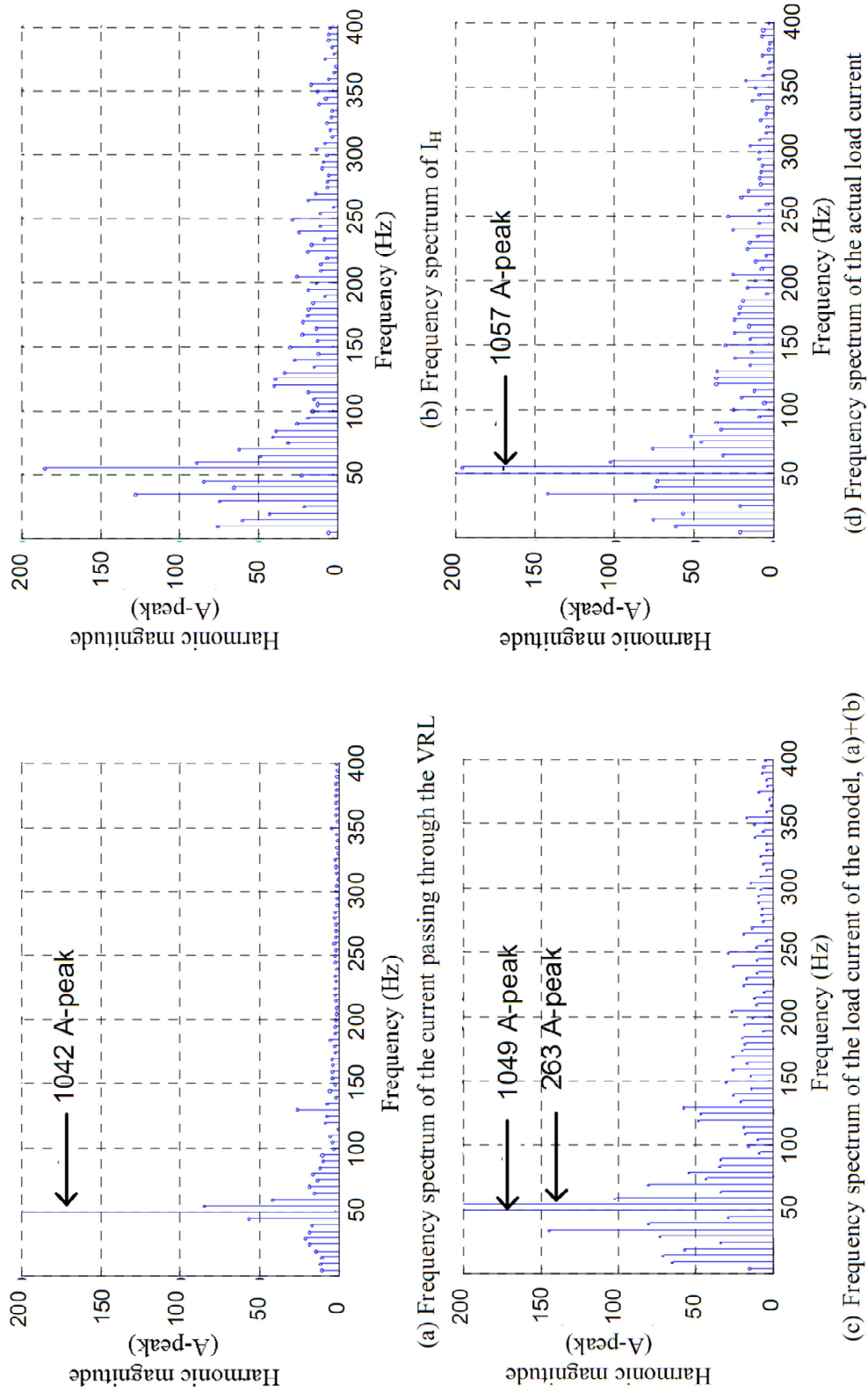
Figure 3.7   Harmonic comparison of the spectra of the actual load current with the spectra of the simulation results.

3.3 Step 3: Verification of the EAF Model When Internal Grid Voltages at VP are Deduced from Voltage and Current Measurements at MP1

In this step, measurements taken at Plant-2 are used again. Measurements are carried out at MP1 in Figure 3.1. Internal voltages, V_s, of the utility grid are then generated by referring voltages at MP1 to VP and the model is excited at VP with the computed voltages. The three-phase detailed model of the existing SVC at that plant is then integrated to the model in EMTDC/PSCAD environment as shown in Figure 2.4. The simulation program is run to obtain the EAF currents and voltages at MP1. It has been found that the measured and the calculated voltage and current values are highly correlated. P and Q variations of six minutes obtained from both measured and computed (using the proposed model) voltage and current data at MP1 for Plant-2 are given in Figure 3.8 for comparison purposes. The measured and computed P and Q variations are nearly the same. In order to quantify how close the computed data relate to the measured data, the corresponding energies (MW-h and MVAr-h) are also shown on the associated power plots in Figure 3.8. It has been found that the measured and the calculated energies are significantly close.

Short term flicker (P_{ST}) values are also computed at MV load bus (34.5 kV line-to-line) for all five plants and they are compared with measured flicker values. Some sample results at MV EAF bus for four of the measured EAF plants are given in Table 3.1, which are obtained by disconnecting the existing SVCs from the MV bus. As it can be understood from the results in Table 3.1, with the proposed model, simulation results give flicker values very close to the measured flicker values at MP1.
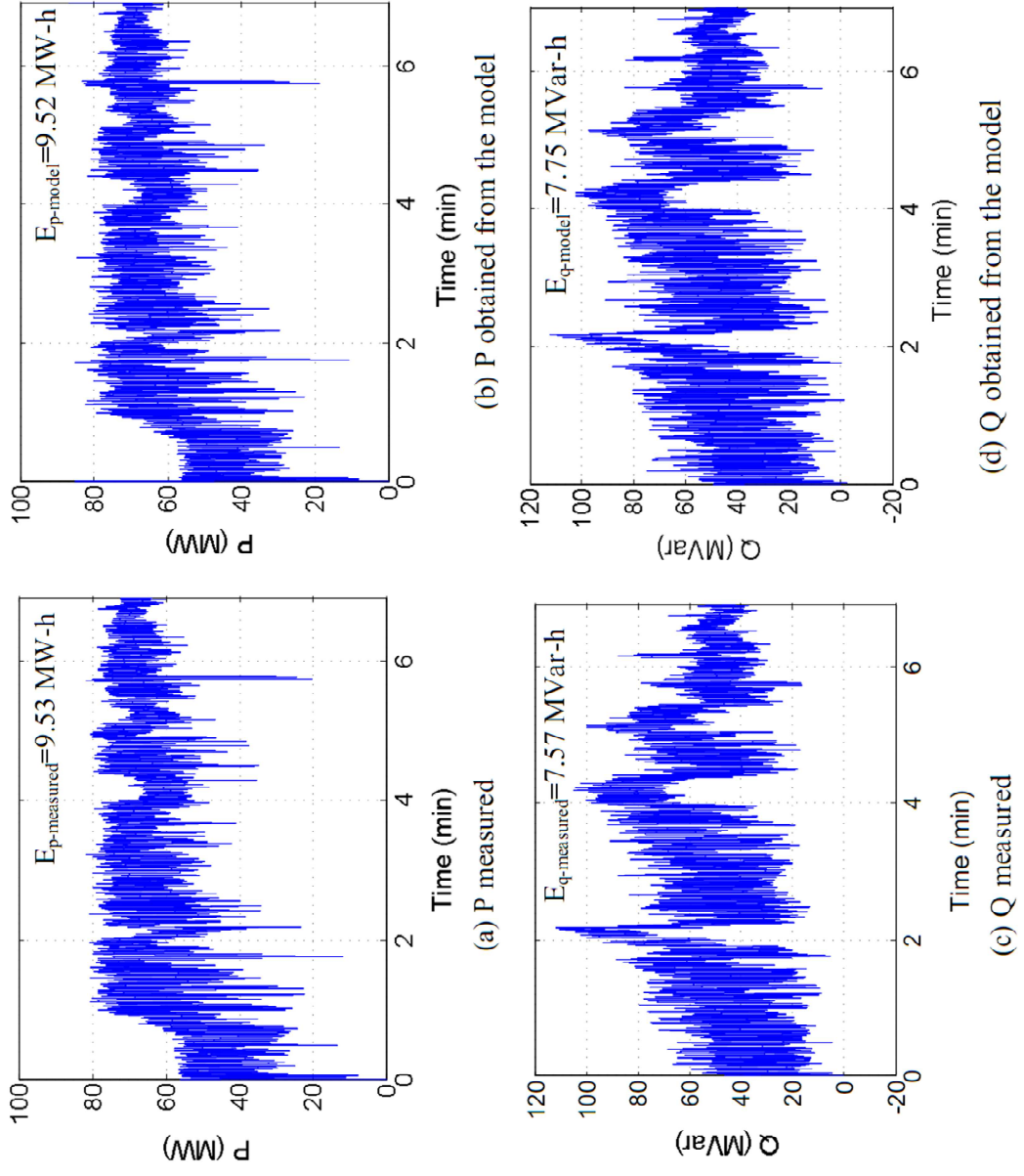
Figure 3.8   Comparison of the measured and computed values of real and reactive powers at MP1.

In this step, the proposed model is run with actual field-data taken at MP3 referred to VP. Simulation results obtained at MP1, using the proposed model are compared with the actual field-data taken simultaneously at the same point. The results constitute a strong verification of the model.

TABLE 3.1   Comparison of the short term flicker results (P_{st}) at MV EAF bus for four EAF plants (Existing SVCs are OFF)

Min	P1 M	P1 S	P2 M	P2 S	P3 M	P3 S	P4 M	P4 S
1	23.43	24.93	15.904	16.392	21.395	20.568	7.304	8.643
2	26.89	27.52	14.708	15.353	19.758	18.984	13.025	13.966
3	33.43	30.87	14.833	15.53	13.879	13.313	12.941	13.702
4	30.92	29.97	ND	ND	14.519	14.798	11.488	11.916
5	22.29	22.82	ND	ND	6.77	6.251	10.193	11.581
6	18.53	20.26	ND	ND	6.413	6.067	9.482	12.583
7	20.18	22.55	ND	ND	2.473	3.739	9.52	12.109
8	25.24	23.00	ND	ND	3.29	4.843	ND	ND

P: Plant; M: Measured; S: Simulated; ND: No Data

3.4 Step 4: Verification of the EAF Model When Internal Grid Voltages at VP are Deduced from Voltage and Current Measurements at MP3

The proposed model is run (with the SVC model of the plant integrated) using EMTDC/PSCAD and the simulation results obtained at the EAF transformer primary (MP1) are compared with those from field measurements at MP1 during boring, melting and refining periods.

The results obtained are found to be very close to each other as given in Figure 3.9. Measured P and Q, and those that are obtained at MP3 by simulation are given in Figure 3.10. Both Figure 3.9 and 3.10 support the fact that the proposed method gives very accurate results.

3.5 Step 5: Verification of the EAF Model by Exciting the System at VP with Rated Value of Internal Grid Voltages V_S

Both the rms value and the frequency of three-phase internal grid voltages are assumed to be constant at their rated values (say 89 kV line-to-neutral and 50 Hz). However, in practice these are changing between maximum and minimum permissible values. Figure 3.11 shows the variations in rms value of line-to-neutral internal grid voltage in comparison with its rated value. Furthermore, the constructed data array for internal grid voltages is not synchronized with the EAF model in time, resulting in asynchronous simulation. The system given in Fig 3.1 is then excited at VP with an asynchronous constant rms voltage data array and the simulation is run to obtain the electrical quantities at MP1. Rms voltage, rms current, P, Q (1-min. averages) obtained at MP1 are given in Figure 3.12 to compare the results with the measured quantities at MP1. Results show that if the internal grid voltage is inside tolerable limits, any measured data at MP3 either synchronous or not are not required for quite accurate results. The same comparison in terms of short term flicker is also given in Figure 3.13. The proposed EAF model obtained at MP1 excited with a constant internal grid voltage at VP gives fairly good results in terms of electrical quantities. This proves the ability of the proposed model to be a practical tool for simulations.
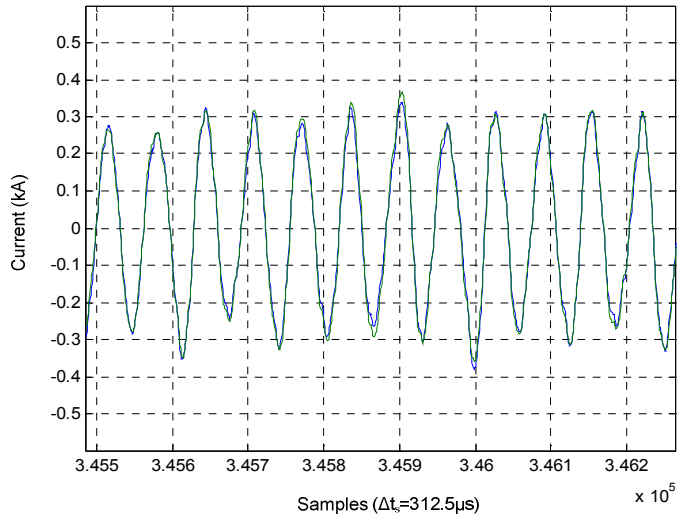
(a) Boring
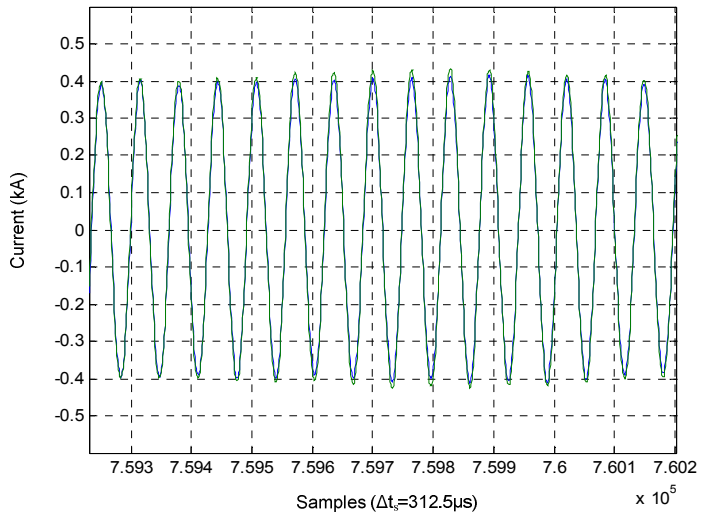
(b) Melting
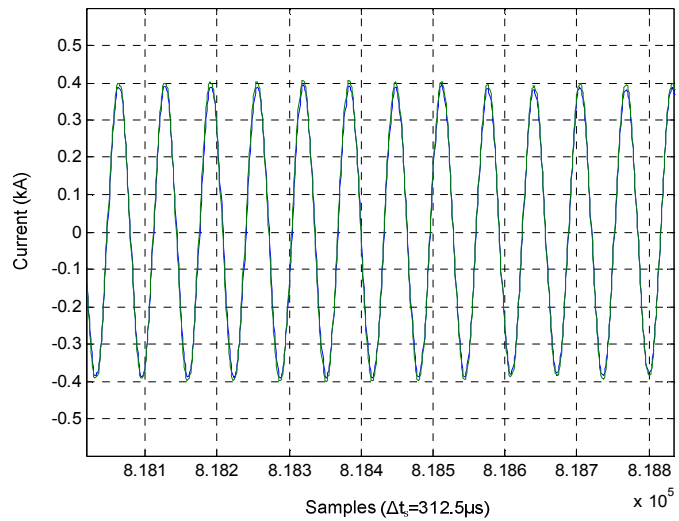
(c) Refining

Figure 3.9   Actual current at MP3 and simulation results plotted together.

$\overline{E}_{p\text{-measured}} = 5.43 \text{ MW-h}$

(a) P measured

$\overline{E}_{p\text{-model}} = 5.64 \text{ MW-h}$

(b) P obtained from the model

$\overline{E}_{q\text{-measured}} = 7.68 \text{ MVAr-h}$

(c) Q measured

$\overline{E}_{q\text{-model}} = 7.37 \text{ MVAr-h}$

(d) Q obtained from the model
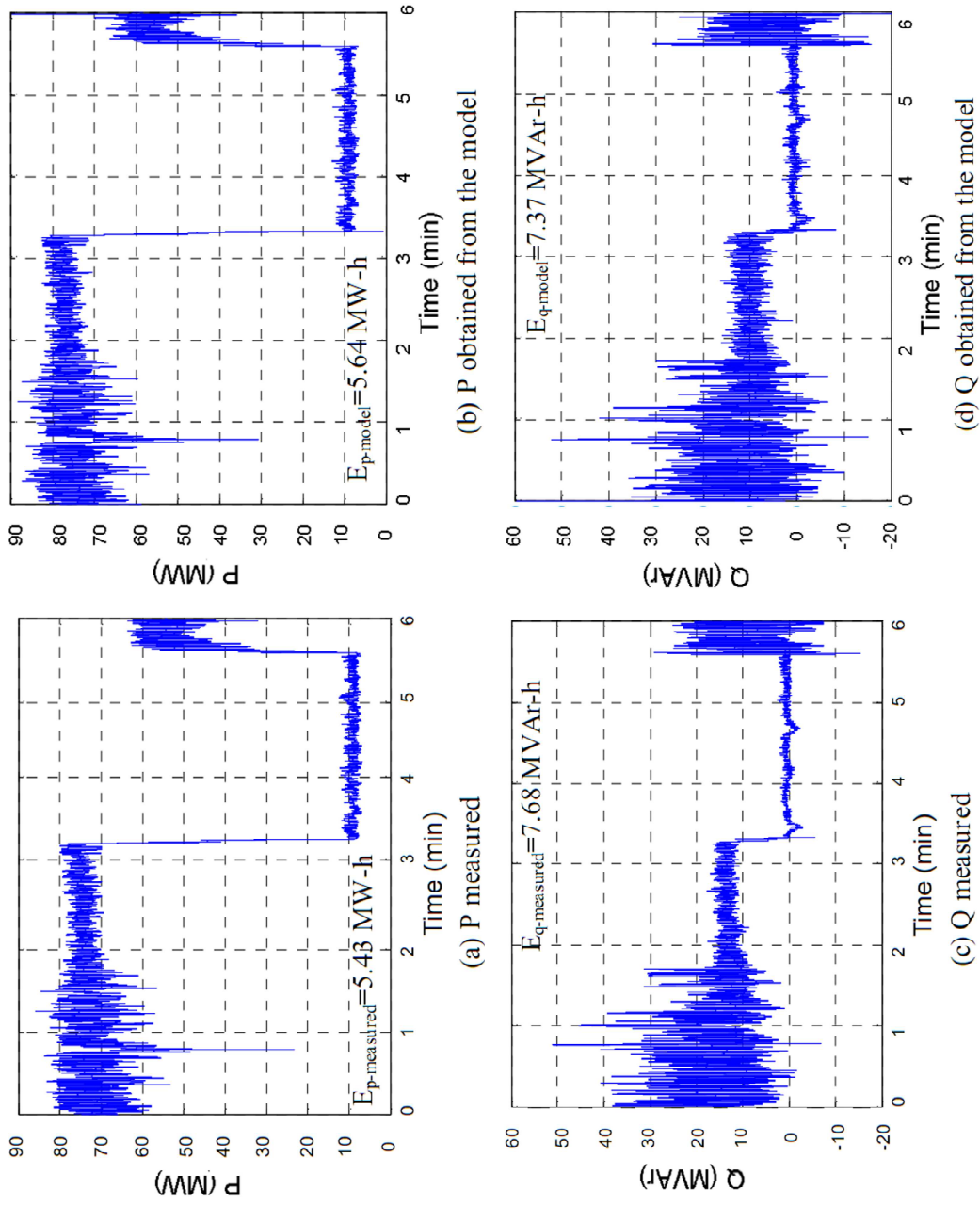
Figure 3.10   Real and reactive powers at MP3.
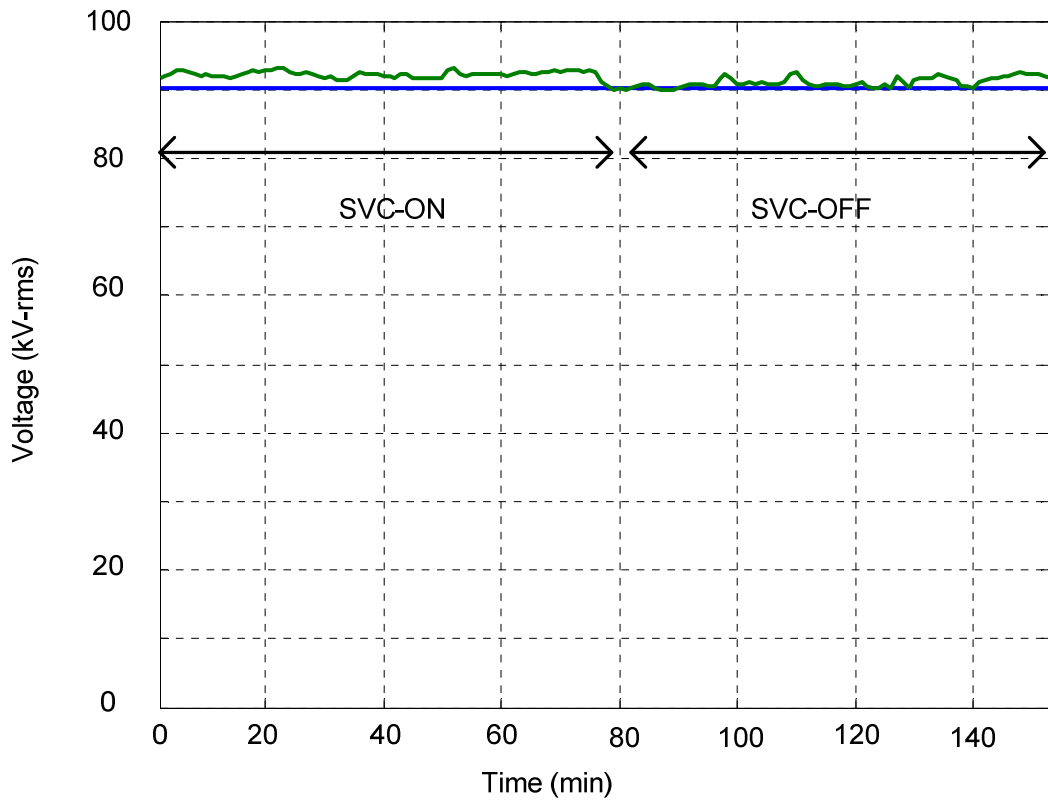
Figure 3.11   Variations in rms value of line-to-line internal grid voltage compared with its rated value (89 kV line-to-neutral).
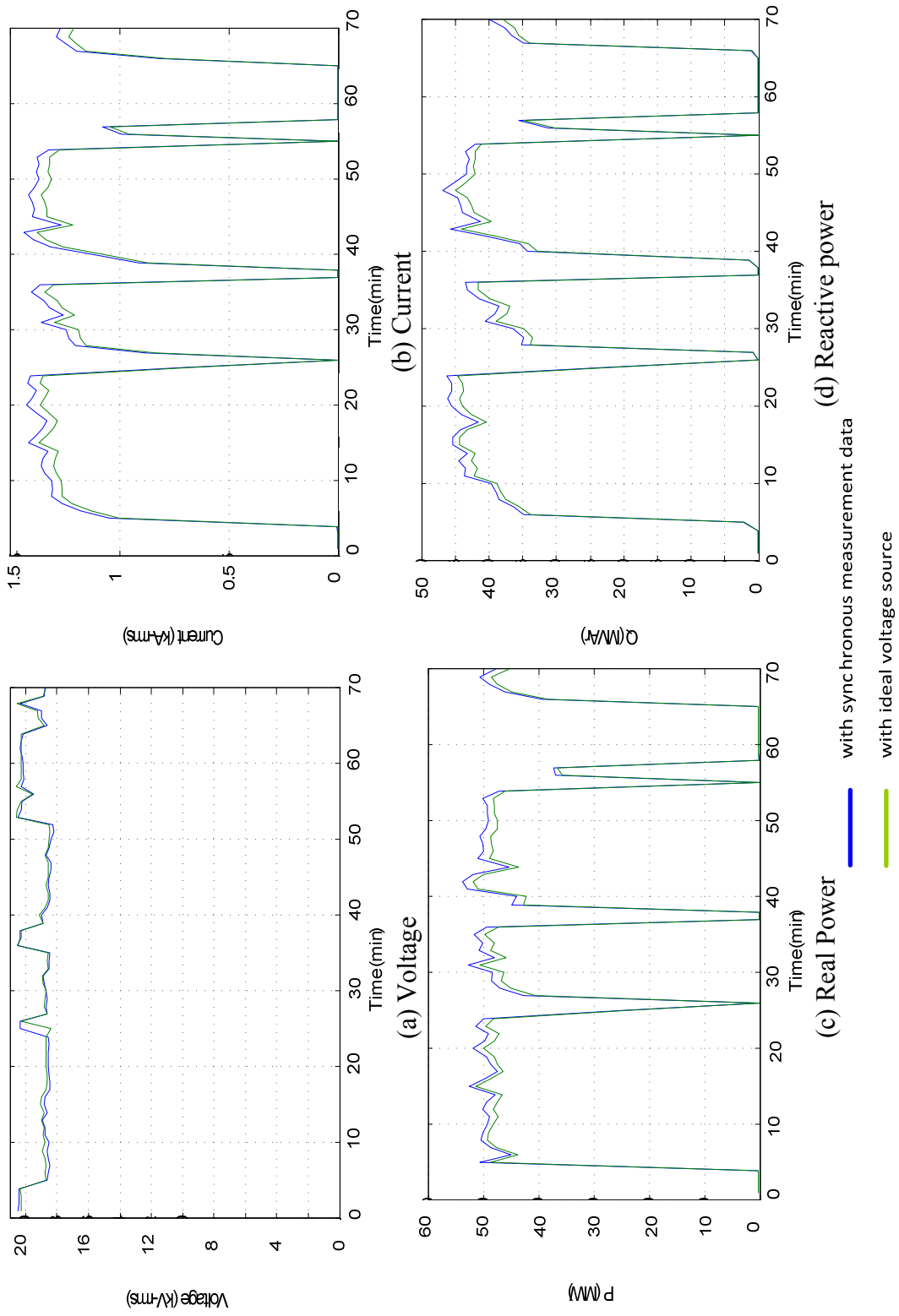
Figure 3.12   Electrical quantities at MP1, comparison of simulation with the proposed model and the measured quantity.
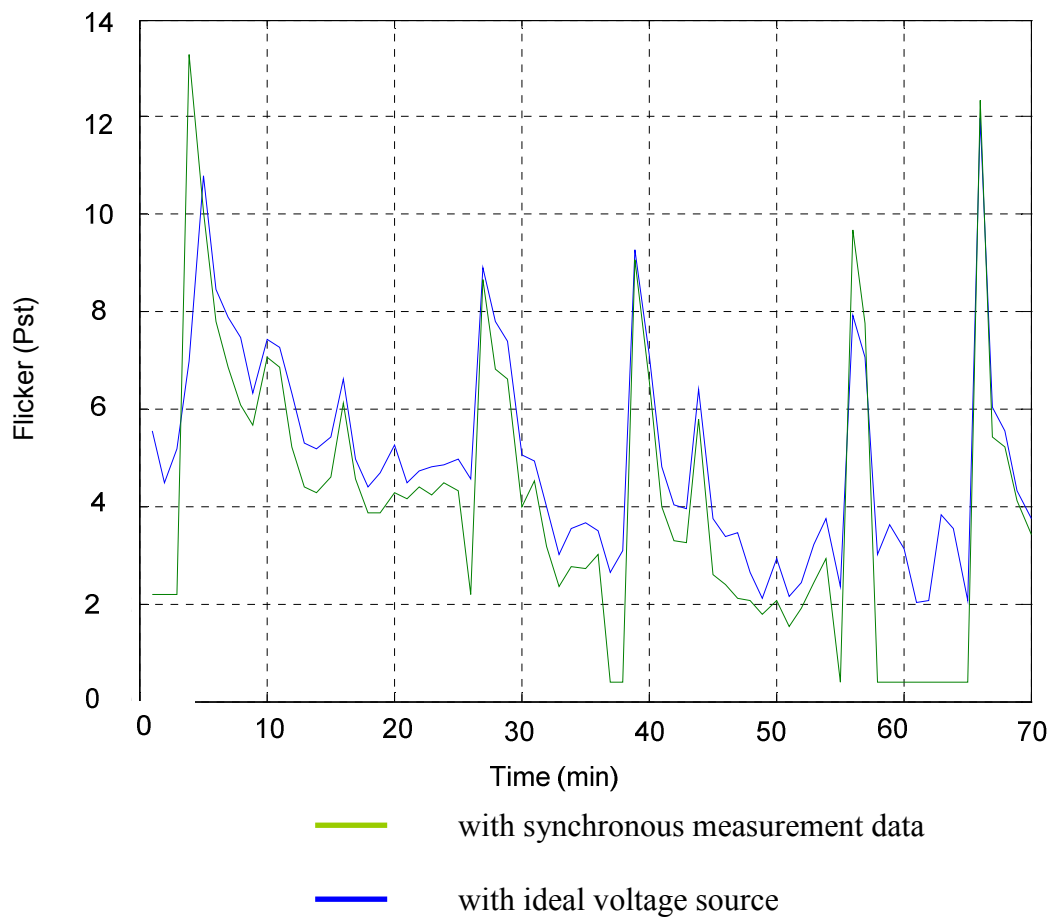
Figure 3.13   Short term flicker, P_{ST}, at MP1.

CHAPTER 4

APPLICATIONS WITH THE MODEL

The results of the verification steps in Chapter 3 have shown that the proposed model can be used as an important design tool to improve the PQ of a single EAF or multi-EAFs connected to a PCC, since it is capable of representing the EAF characteristics satisfactorily. This chapter will present four applications of the model with various cases, provide the results obtained, and compare them with the expected results.

To mitigate the PQ problems, FACTS devices such as TCR based SVCs, STATCOMs, APFs, and etc. can be connected to the MV EAF bus or existing SVCs can be upgraded. Since the performances of the FACTS devices on reactive power compensation and harmonic filtration are already known, applications employed in this chapter focus on the effects of the FACTS devices on the reactive power compensation and the harmonic filtration besides the short term flicker (P_{ST}) variations.

4.1 Single-Furnace Operation without Compensation

There are two types of multi-furnace operations. Either the EAFs are connected to a common MV bus, such that they belong to the same plant, or to a common HV bus, such that they belong to different plants but those plants are connected to the same power grid as in Turkey. Figure 4.1 shows a sample single-line diagram for a multi-furnace operation with a single plant. The SVC in Figure 4.1 is the simulation of the actual SVC system used by the plant of EAF1. The models of EAF1 and EAF2 are acquired through the proposed EAF modeling method described in Chapter 2.
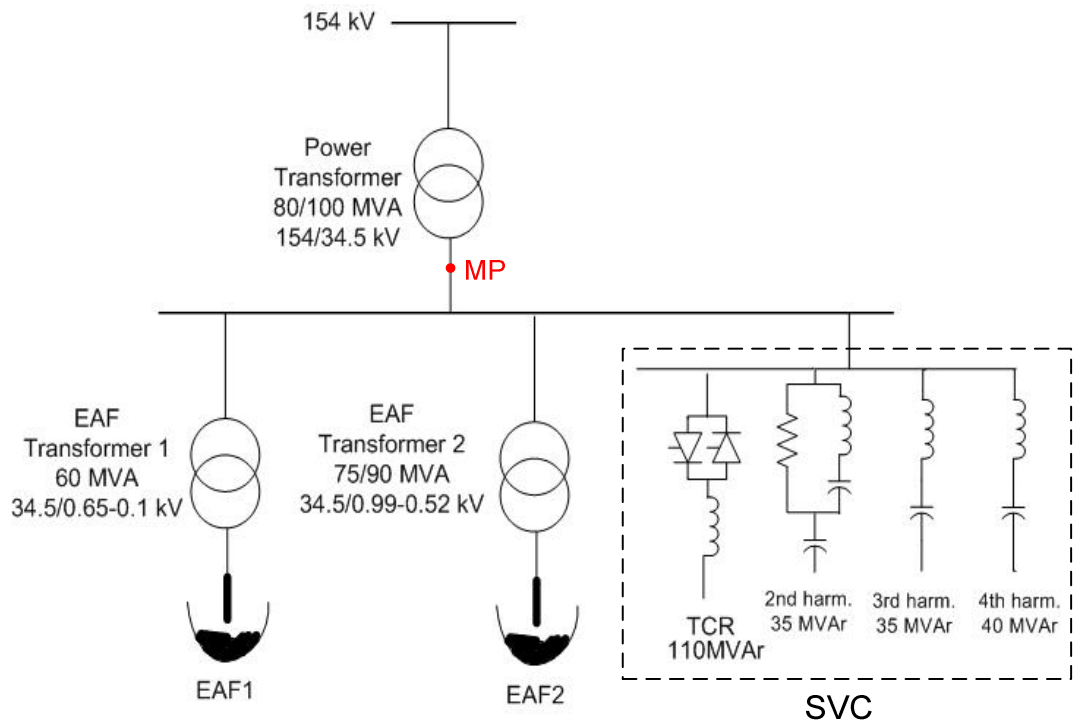
Figure 4.1   Single-line diagram of multi-furnace operation with SVC.

This subsection investigates the single-furnace operation without any compensation, therefore, the SVC and the EAF2 models in Figure 4.1 are switched off during the simulation. EAF1 is in the melting phase during the first 150 seconds and it is in the refining phase during the last 150 seconds in the simulation. Figure 4.2 and Figure 4.3 show the active and the reactive power, and the second, third, fourth and the fifth harmonic variations at the MV side of the power transformer in Figure 4.1 (MP-measurement point) respectively.
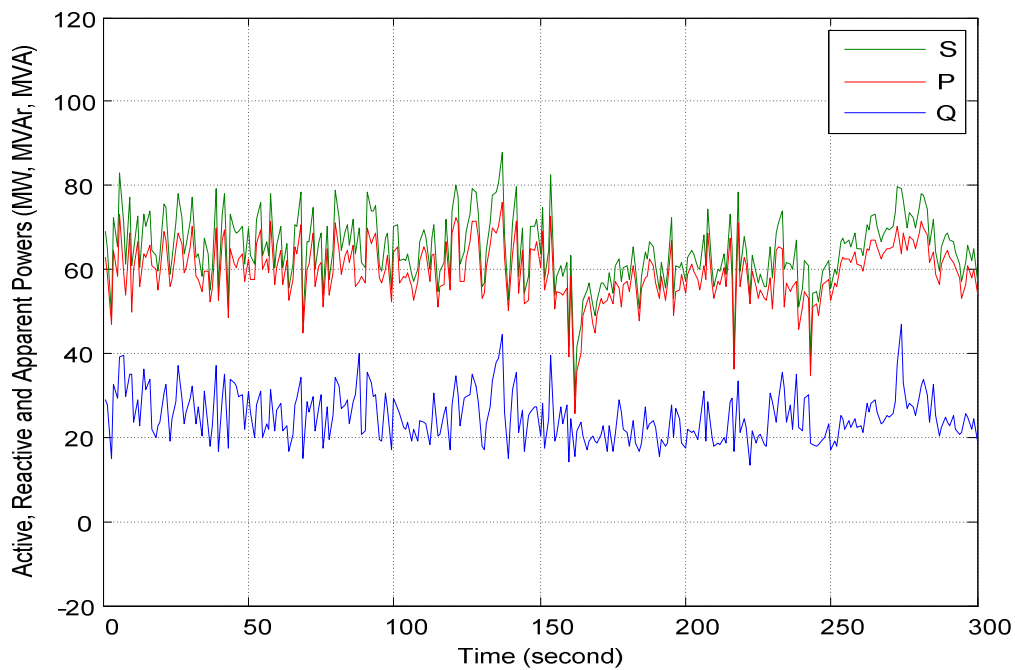
Figure 4.2   Active, reactive and apparent power variations at the MV side of the power transformer when EAF1 is in operation and SVC and EAF2 are OFF (MP, 1-sec averages).

(a) 2nd Harmonic
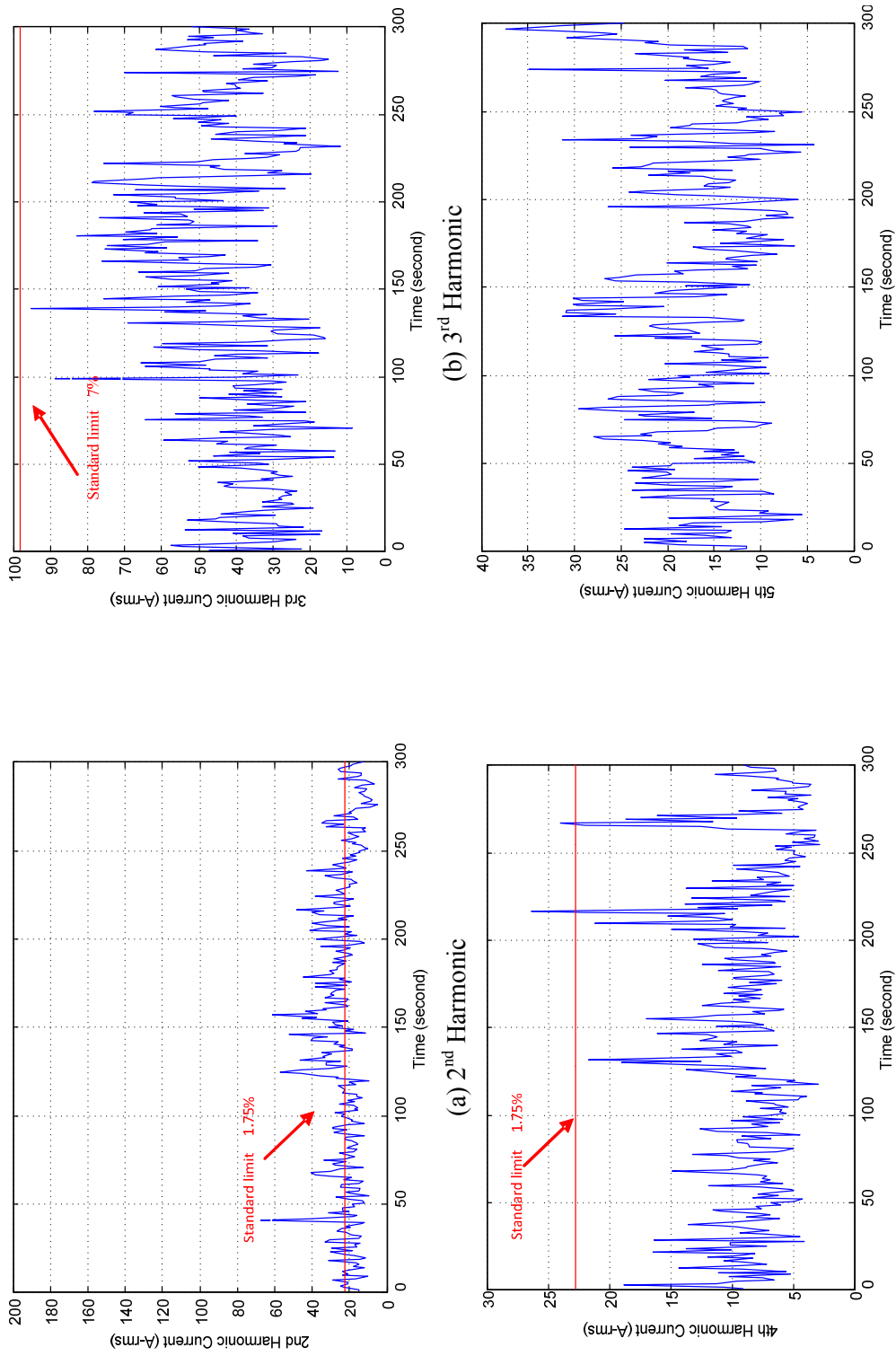
(b) 3rd Harmonic

(c) 4th Harmonic

(d) 5th Harmonic (standard limit is 7%, 97 A-rms)

Figure 4.3   Line current harmonics variation at MV side of the power transformer (MP, 1-sec averages).

47

Red lines in Figure 4.3 represent the allowed harmonic current limits determined by the Electricity Transmission System Supply Reliability and Quality Regulation [23]. Harmonic current limit determination is explained briefly in Appendix D.

4.2 Single-Furnace Operation with SVC

Single-furnace system is operated with the SVC model given in Figure 4.1. EAF1 is in operation and EAF2 is OFF. Figures 4.4 and 4.5 show the obtained results at MP in Figure 4.1. Comparing the results of the subsection 4.1 and 4.2 (i.e. Figure 4.3 and 4.4); it is observed that SVC is effectively used for the reactive power compensation, and the filtration of the third, fourth and the fifth harmonics. It should be noted that the second harmonic content of the current at MP is increased when the SVC is in operation, because the frequency response of the harmonic filters amplify the spectral content around the second harmonic. As seen from Figure 4.6, the frequencies lower than 132 Hz, and the frequencies between 169 and 179 Hz especially are amplified.

Figure 4.4   Active, reactive and apparent power variations at the MV side of the power transformer (MP, 1-sec averages).
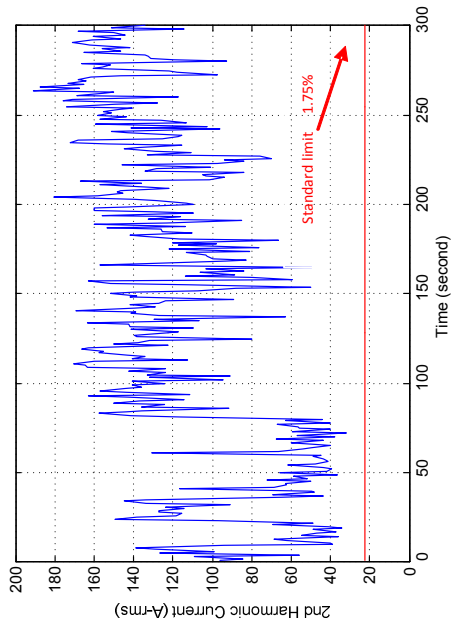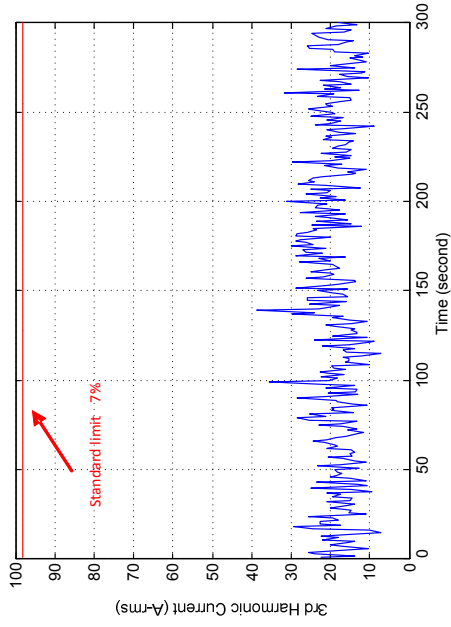
(a) 2nd Harmonic

(b) 3rd Harmonic
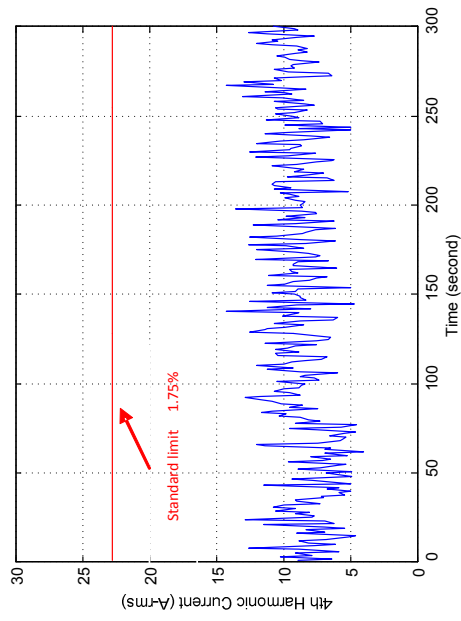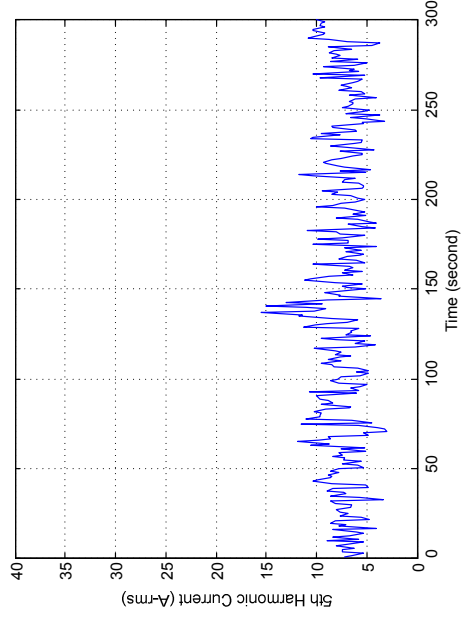
(c) 4th Harmonic

(d) 5th Harmonic (standard limit is 7%, 97 A-rms).

Figure 4.5   Line current harmonics variation at MV side of the power transformer (MP, 1-sec averages).
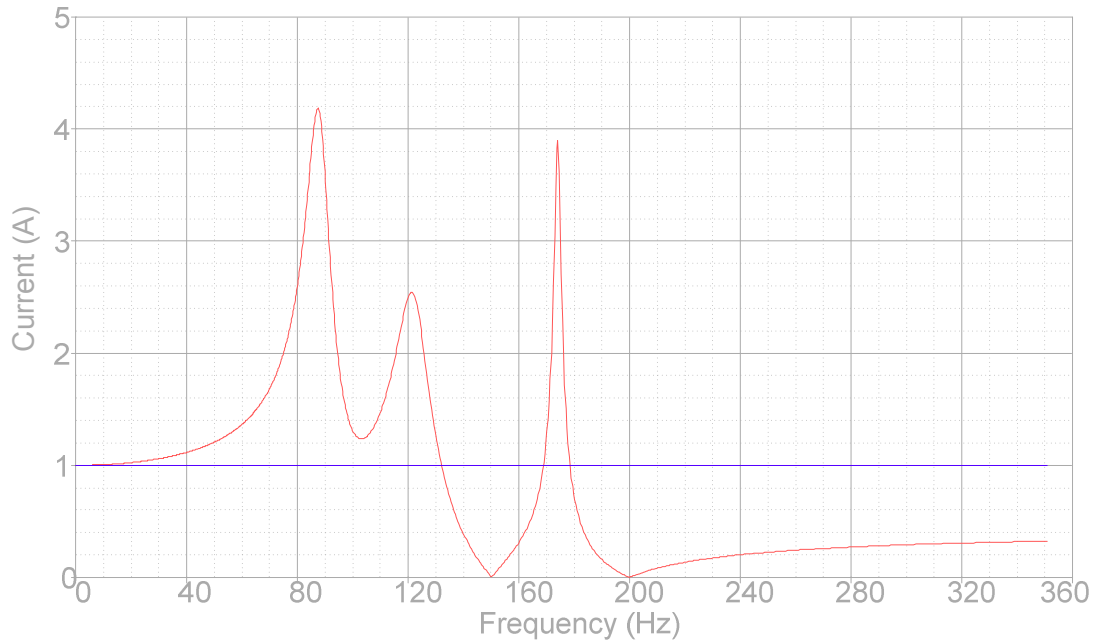
Figure 4.6   Frequency response of the harmonic filters in Figure 4.1.

The frequency response in Figure 4.6 is obtained by simulating the single-phase circuit given in Figure 4.7 with OrCAD simulation tool. The circuit is the single-phase equivalent of the exact three-phase passive harmonic filters drawn by a current source. There is no voltage source since 50 Hz is not considered. R_S and L_S represent the source impedance at the MV side of the power transformer in Figure 4.1. The circuit is excited by AC sweep method, such that one-ampere-rms-amplitude sinusoidal current sweeps the frequency range from one Hz to 360 Hz with one Hz increments. The frequency response is obtained as the magnitude of I_S in A-rms when the circuit is excited by the current source given in Figure 4.7.
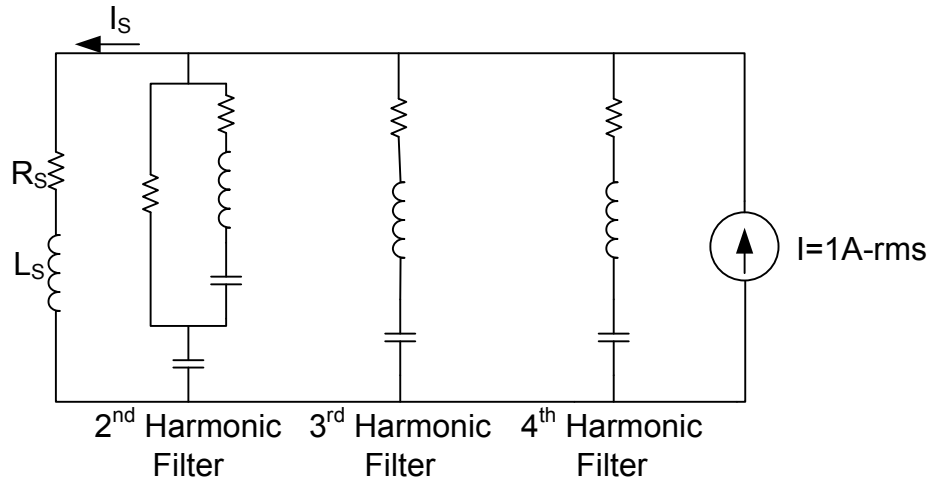
Figure 4.7   Circuit diagram to obtain the frequency response of the harmonic filters in Figure 4.1.

4.3 Multi-furnace Operation with SVC

In this subsection, the compensated multi-furnace operation is simulated with EAF1, EAF2 and the SVC all in operation, and the obtained results are presented in Figures 4.8 and 4.9. EAF2 is in the boring phase during the first 160 seconds and it is in the melting phase during the last 140 seconds. When results are investigated, it is observed that SVC has a sufficient performance on the reactive power compensation and the filtration of the third, fourth and the fifth harmonics. But as in subsection 4.2 (single-furnace operation with SVC), the second harmonic content is increased due to the frequency response of the harmonic filters.
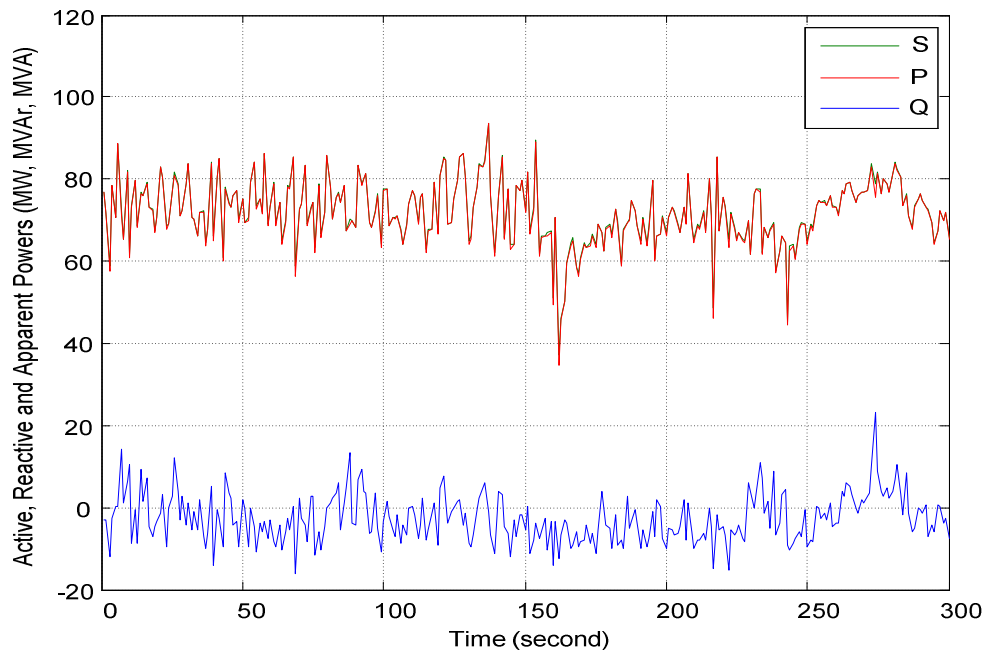
Figure 4.8   Active, reactive and apparent power variations at MV side of the power
transformer (MP, 1-sec averages).

(a) 2nd Harmonic

(b) 3rd Harmonic(standard limit is 7%, 117 A-rms)

(c) 4th Harmonic

(d) 5th Harmonic (standard limit is 7%, 117 A-rms

Figure 1.9   Line current harmonics variation at MV side of the power transformer (MP, 1-sec averages).

Five different case studies are carried out on the multi-furnace system as described in Table 4.1 to present the flicker variations for the uncompensated single-furnace operation, the single-furnace operation with SVC and the multi-furnace operation with SVC. Sample short term flicker P_{ST} variations for these case studies are as presented in Figure 4.10.

Figure 4.10   Short term flicker at MV bus supplying EAFs.

TABLE 4.1   Case studies on multi-furnace operation given in Figures 4.1 and 4.10

Case	EAFs		SVC	
	EAF1	EAF2	TCR	Harm. Filters
a	ON	ON	ON	ON
b	ON	OFF	ON	ON
c	ON	OFF	OFF	ON
d	ON	OFF	OFF	OFF

The following conclusions can be drawn from the P_{ST} variations given in Figure 4.10:

i)   The lowest P_{ST} values have been obtained for Case-d in which only EAF1 is operating in an uncompensated manner (SVC-OFF).

ii) Connection of harmonic filters to the MV (34.5 kV) bus does not make a significant change in P_{ST} values (Case-c).

iii) Activation of the SVC cannot make any contribution in reducing P_{ST} values as expected [21], but causes a slight increase in P_{ST} values (Case-b).

iv) Putting the EAF2 into operation in addition to the EAF1 leads to a further increase in P_{ST} as shown in Case-a of Figure 4.10.

v)   New flicker mitigation technologies together with or without the existing SVC are to be exercised in order to bring flicker values to acceptable limits especially at HV (154 kV) bus.

This model can also be used satisfactorily to predict all PQ parameters of the EAF for various operating conditions, as well as multi-furnace EAF operation with various PQ conditioner systems.

4.4 Single-furnace Operation with APF

In this application, instead of a TCR based SVC to mitigate PQ problems of an EAF, an APF is employed. APF is a converter-based FACTS device which aims to inject the current with a desired wave shape. Therefore, an APF can both filter out the harmonics in load current and compensate the reactive power demand of the load.

The APF in Figure 4.11 is designed for both reactive power compensation and harmonic filtration. The single-line diagram of the EAF-APF system is as shown in Figure 4.11. APF is designed to filter out the whole frequency spectrum of the EAF current except the fundamental frequency in the simulation environment.
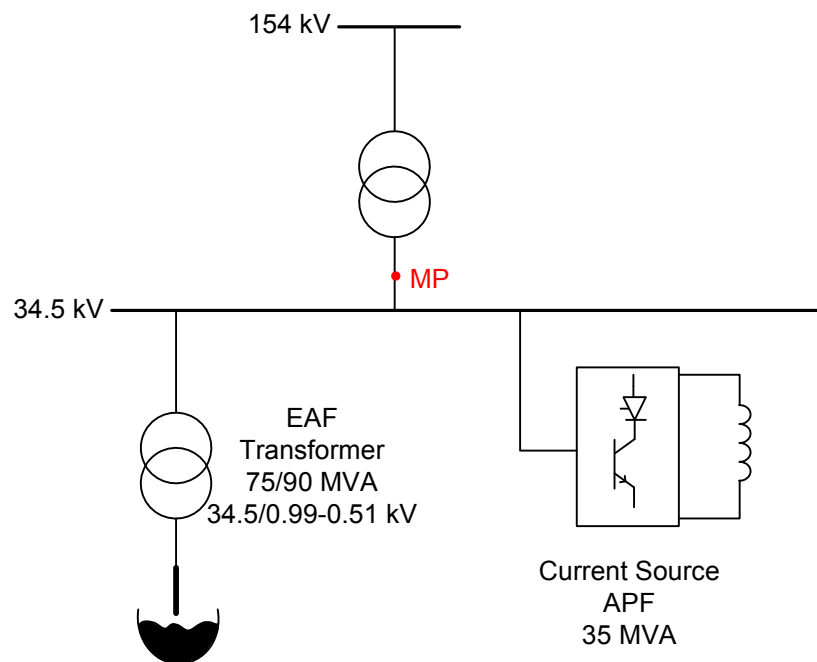
Figure 4.11   Single-line diagram of single-furnace operation with APF.

The system was operated for two cases in the simulation environment. First, uncompensated system is simulated, and then the system compensated with the APF is simulated for the cases mentioned in Table 4.2 to see the performance of the APF on flicker mitigation. Results obtained in the sense of P_{ST}, reactive power compensation and harmonic filtration are presented in Figures 4.12, 4.13 and 4.14, respectively.

Figure 4.12 shows that an APF can also be used instead of a TCR based SVC for reactive power compensation. Although the whole harmonic content of the line current at the MV side of the power transformer cannot be reduced under the limits, Figure 4.13 shows that APF has filtered out all of the harmonic currents up relatively compared to the SVC. The results given in Figure 4.14 show that an APF filtering the whole unwanted harmonic and interharmonic content of the EAF current spectrum decreases the P_{ST} of the power grid.
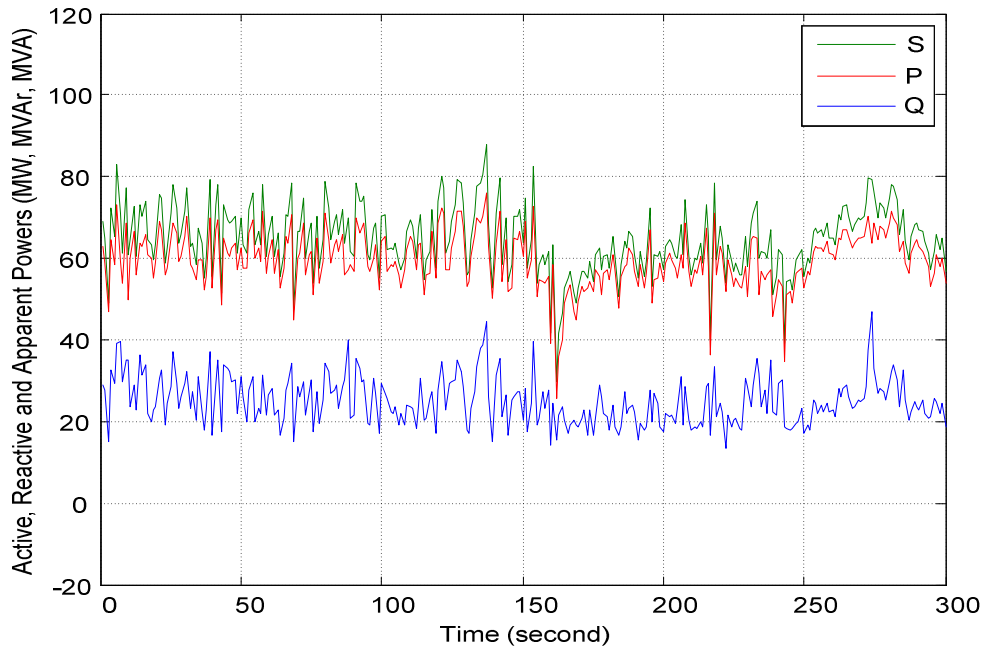
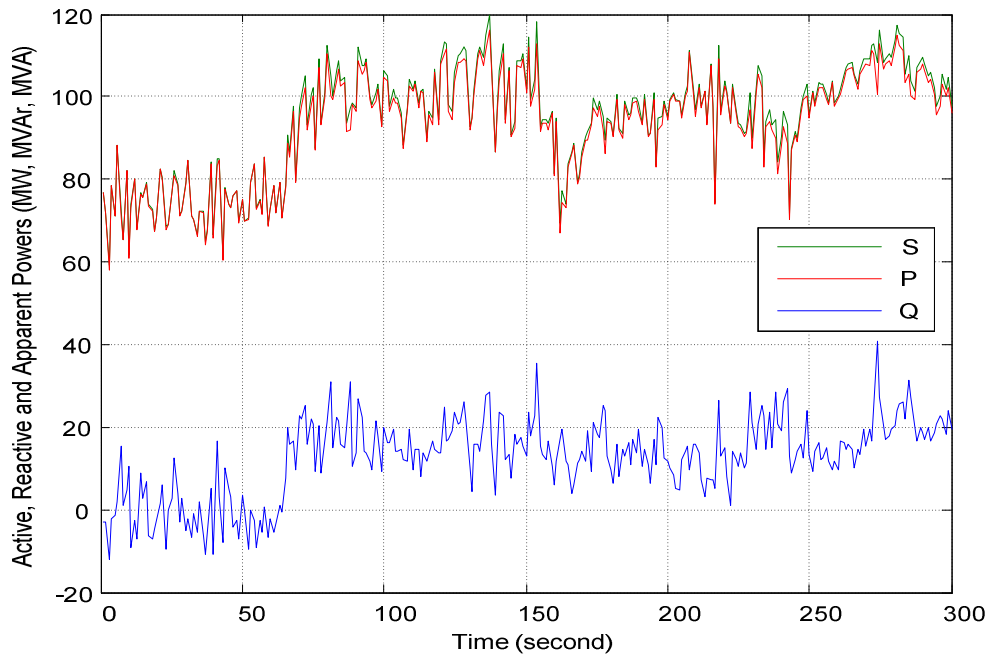(a) without compensation
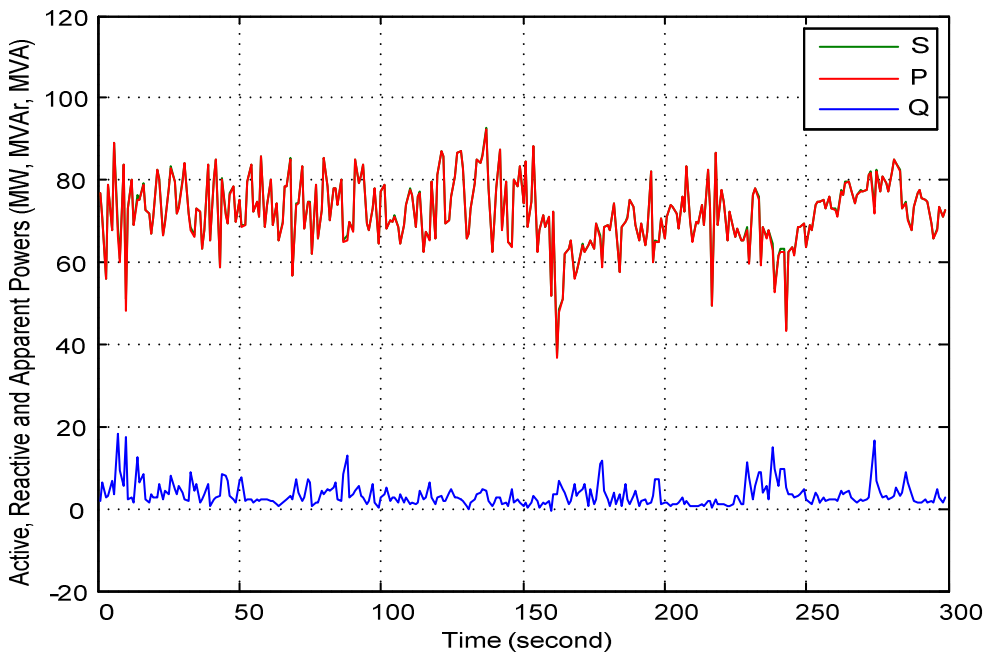
(b) with APF

Figure 4.12   Active, reactive and apparent power variations at MV side of the power
transformer (MP, 1-sec averages).
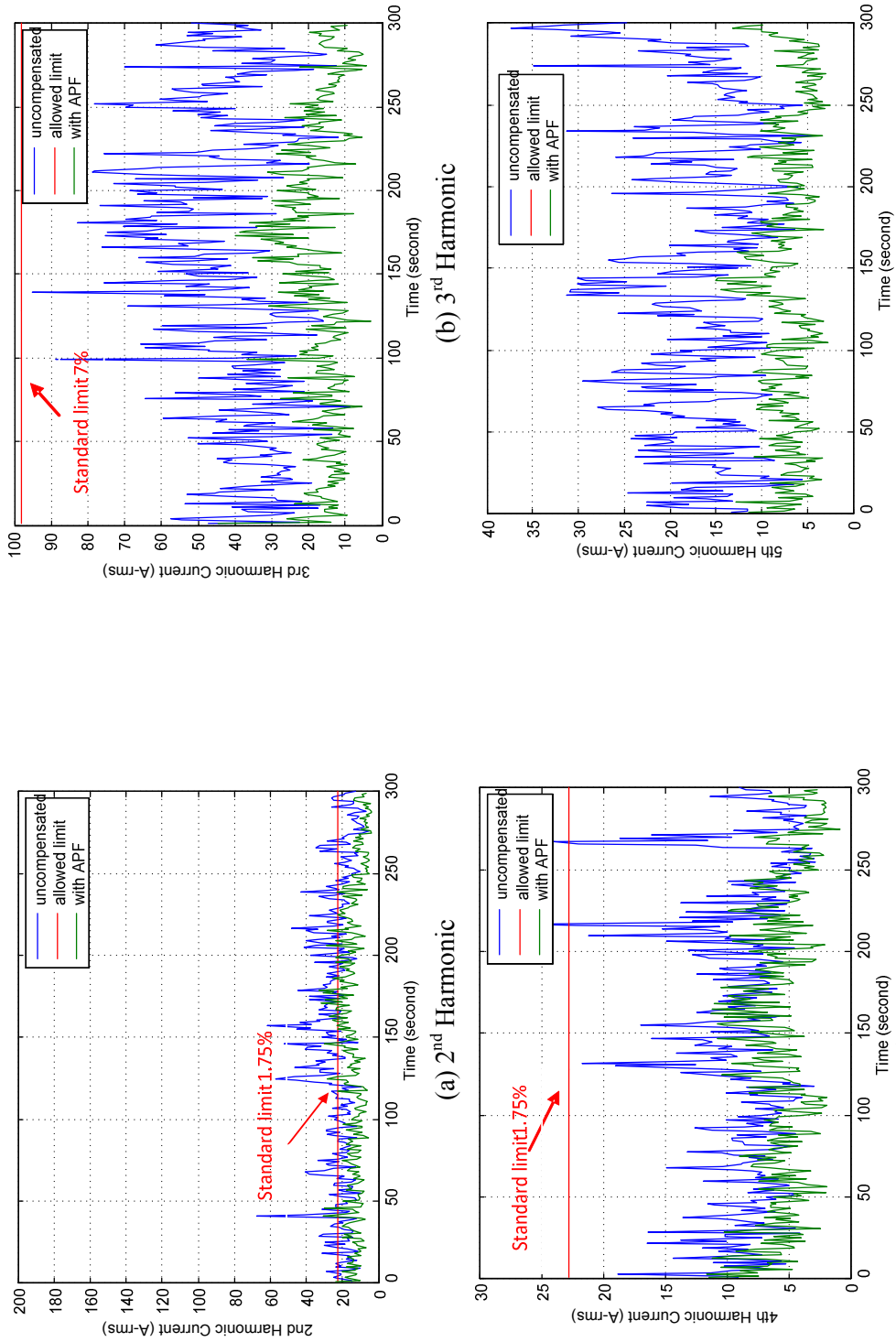
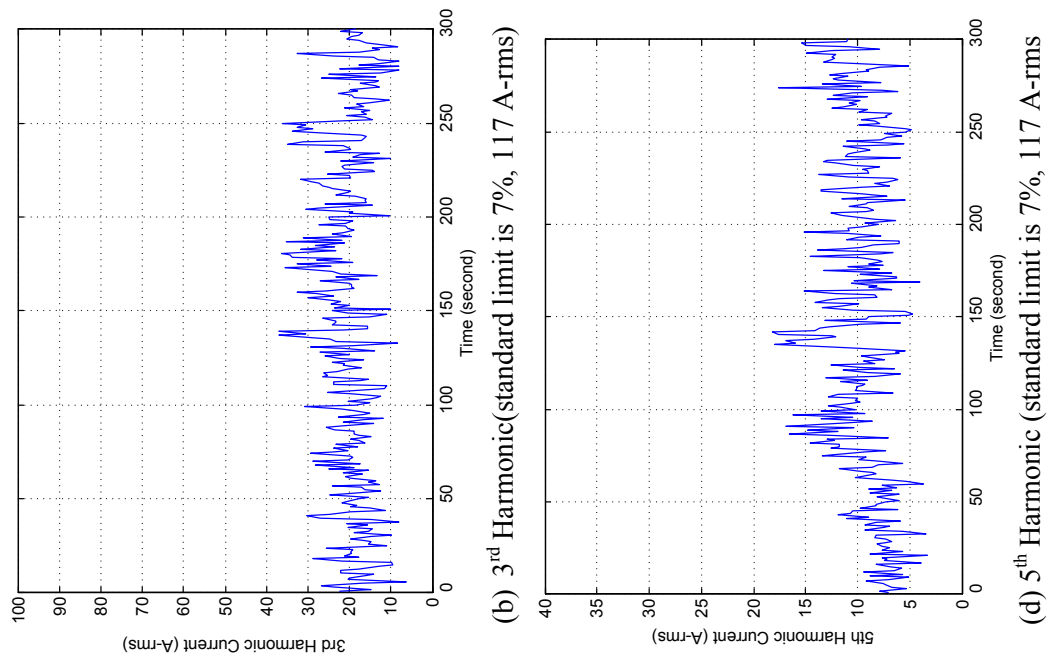Figure 1.13   Line current harmonics variation at MV side of the power transformer (MP, 1-sec averages).
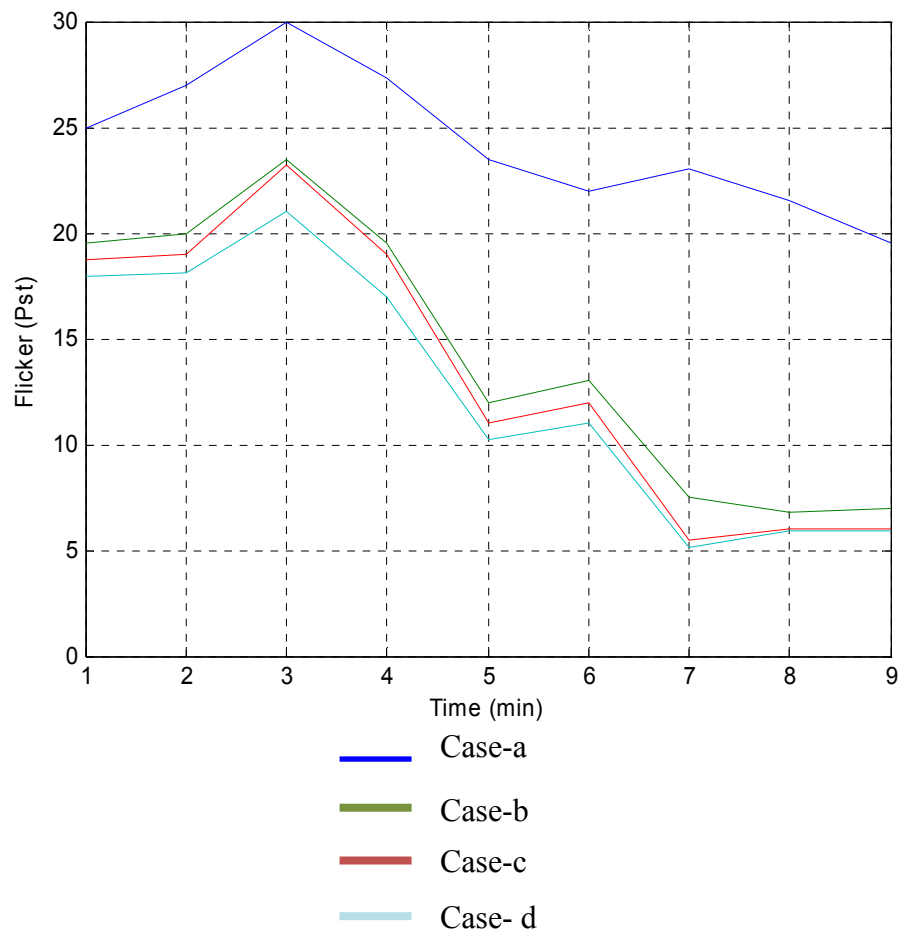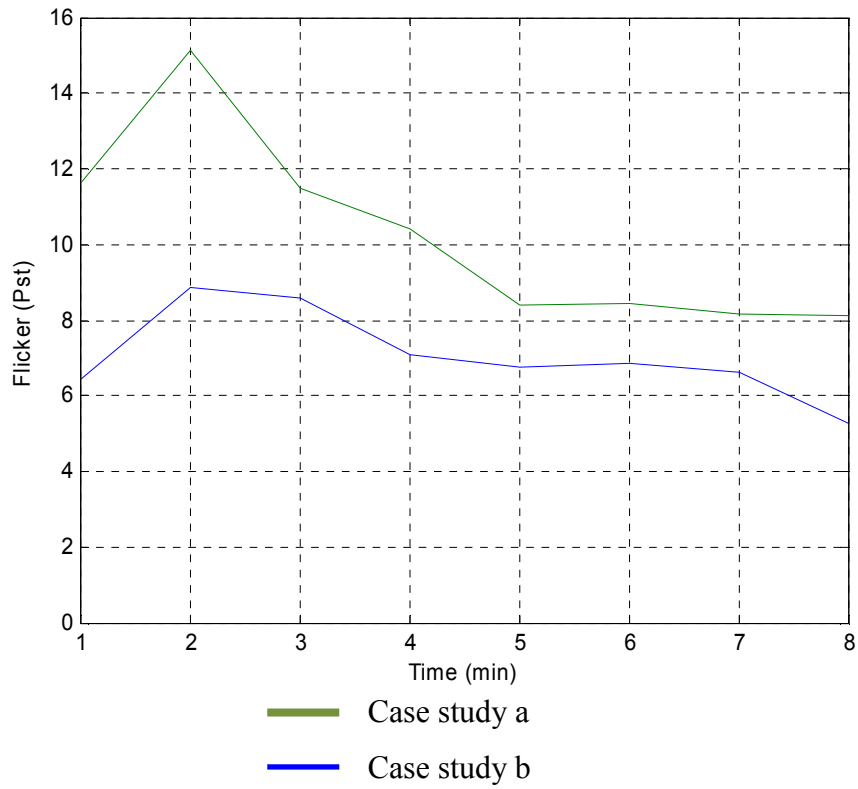
Figure 4.14   Short term flicker at MV bus supplying EAFs.

TABLE 4.2   Case studies on EAF-APF operation given in Figures 4.11 and
4.14

Case	EAF	APF
a	ON	OFF
b	ON	ON

4.5 Discussion on the Results of the Applications with the Model

Single-furnace operation without compensation shows that the EAFs have seriously inverse effect on the electrical power systems in terms of PQ as seen in Figures 4.2 and 4.3. When the SVC, which is the major device used for reactive power compensation of the EAFs, is taken into operation to compensate the single-furnace operation, it has been observed that the reactive power compensation is fully achieved as seen in Figure 4.4. Although the second harmonic component is amplified due to the frequency response of the passive filters, harmonic filtration is also obtained successfully for the third, fourth and the fifth harmonics as seen in Figure 4.5. Short term flicker is also increased due to the second harmonic amplification which can be concluded from Case-b and Case-d of Figure 4.10. Compensating the multi-furnace operation with the same SVC is not as satisfactory as single-furnace operation with SVC as expected. Reactive power is compensated up to acceptable limits as shown in Figure 4.8. SVC's performances on harmonic filtration and flicker are similar as in the case of single-furnace operation with SVC. It can be concluded that reactive power demand of the EAF can be compensated with the SVC, if the SVC has proper rating. SVC can be used for filtration of harmonics greater than the second harmonic, but SVC amplifies the second harmonic and increases the short term flicker due to frequency response of the passive filters.

Applications show that the APF has a better performance in the reactive power compensation and the harmonic filtration of a single-furnace EAF system, compared to the SVC. Figures 4.12 and 4.13 present the results of the reactive power compensation and the harmonic filtration. Figure 4.14 also shows that the APF is effective on flicker mitigation. However the required rating of the APF is so high that it is too expensive to realize it.

CHAPTER 5

CONCLUSIONS

A new EAF-specific model, dedicated to assessment and mitigation of PQ problems has been proposed in this thesis. The model is based on field measurements of the EAF system obtained at the primary side of the EAF transformer, which includes the EAF transformer and electrode movements besides the EAF itself. The proposed model is applicable to the power quality (PQ) analysis of a new EAF and/or a FACTS device installation, and/or a multi-furnace EAF operation at a certain point of common coupling, since it has been observed that the impedance characteristics of a specified EAF system does not vary significantly for different operating conditions, although the arc resistance of the EAF has a stochastic behavior. The model is specifically useful to determine the PQ variations and flicker primarily, and the harmonic quantities secondarily. In particular the following conclusions can be derived from the results obtained throughout the thesis work:

- The proposed model is capable of reflecting the voltage dependent current behavior of the EAF system by using a variable resistance and inductance (VRL) model.

- Deriving the model by assuming constant power frequency of 50 Hz is employed and it is concluded that determining the exact frequencies of each cycle for the VRL and the harmonic current computation is an important task to obtain a satisfactory model.

- Once the EAF model is obtained at the transformer primary, internal grid voltage can be indirectly computed from synchronous measurements obtained at the PCC. In this case, P and Q variations and flicker of the EAF can be computed

with negligible error. The model can be used to predict the effects of dynamic PQ conditioners which are being planned to be connected to the EAF plants. In terms of harmonics and interharmonics, the model also provides useful results.

- The model can be useful to investigate the effects of new EAF installations in multi-furnace plants in the simulation environment. Prediction of PQ in case of a new EAF installation can provide the opportunity to develop solutions to potential PQ problems.

- All PQ investigations for a new EAF or a dynamic power quality conditioner installation can also be achieved with acceptable accuracy using the proposed model by assuming that internal grid voltage is at rated value and rated frequency, without taking simultaneous measurements at the PCC and the EAF transformer primary.

As future-work, the proposed model can be used to develop an EAF-database. Since the model is obtained from field measurements, models with different operating conditions of different EAFs (various capacities, types and etc.) can be stored in the database. Then the worst relevant model from the database can be used for simulation of a new EAF installation or other possible simulation cases.

The common method used for the regulation set-point of the power system of the EAF system is controlling the impedance magnitude of the EAF system. The systems considered during the development of the model also use this method to control the active power consumed. Therefore for the systems whose set-points are the current drawn by the EAF, the model should be re-developed accordingly.

REFERENCES

[1] IEC 61000-4-30, *Testing and Measurement Techniques-Power Quality Measurement Methods*.

[2] IEC-61000-2-2, *Environment-Compatibility Levels for Low-Frequency Conducted Disturbances and Signaling in Public Low-Voltage Power Supply Systems*.

[3] IEC-61000-4-7, *Testing and Measurement Techniques-General Guide on Harmonics and Interharmonics Measurements and Instrumentation, for Power Supply Systems and Equipment Connected Thereto*.

[4] Areva T & D, http://www.areva-td.com, last visited on September 2009.

[5] D. A. Akdağ, C. Alptekin, I. Çadırcı, et. al., *EKDEMİR Elektrik Ark Ocağı Sistemi: Deneysel ve Kuramsal İncelemeler ve Sistem Başarımını İyileştirici Önlemler*: February 1995.

[6] G. T. Heydt, *Electric Power Quality*: Stars in a Circle Publications, Indiana, 1991.

[7] I. Vervenne, K. Van Reusel, R. Belmans, *Electric Arc Furnace Modeling from a "Power Quality" Point of View*: 9th International Conference on Electrical Power Quality and Utilization, pp. 1-6, Barcelona, October 9-11, 2007.

[8] G.W. Chang, Y.J. Liu, C.I. Chen, *Modeling Voltage-Current Characteristics of an Electric Arc Furnace Based on Actual Recorded Data: A Comparison of Classic and Advanced Models*: Power and Energy Society General Meeting, Conversion and Delivery of Electrical Energy in the 21st Century, pp. 1-6, July 20-24, 2008.

[9] E. O'Neill-Carrillo, G. T. Heydt, E. J. Kostelich, et.al., *Nonlinear Deterministic Modeling of Highly Varying Loads*: IEEE Transactions of Power Delivery, vol. 14, no.2, pp. 537 - 542, April 1999.

[10] E. A. Cano Plata, H. E. Tacca, *Arc Furnace Modeling in ATP-EMTP*: International Conference on Power Systems Transient, Montreal, Canada June 19-23, 2005.

[11]   H. Mokhtari, M. Hejri, *A New Three Phase Time-Domain Model for Electric Arc Furnaces Using MATLAB*: Transmission and Distribution Conference and Exhibition 2002, vol. 3, pp. 2078-2083, October 6-10, 2002.

[12]   C. Han, A. Q. Huang, S. Bhattacharya, M. Ingram, *Field Data-based Study on Electric Arc Furnace Flicker Mitigation*: Industry Applications Conference, 41st IAS Annual Meeting, vol.1, pp. 131-136, October 8-12, 2006.

[13]   Omer Ozgun, Ali Abur, *Flicker Study Using a Novel Arc Furnace Model*: IEEE Transactions on Power Delivery, vol. 17, no.4, pp. 1158-1163, October 2002.

[14]   A.R. Sadeghian, J.D. Lavers, *Application of Radial Basis Function Networks to Model Electric Arc Furnaces*: International Joint Conference on Neural Networks, vol.6, pp. 3996-4001, July 10-16, 1999.

[15]   Fenghua Wang, Zhijian Jin, Zishu Zhu, Xusheng Wang, *Application of Extended Kalman Filter to the Modeling of Electric Arc Furnace for Power Quality Issues*: International Conference on Neural Networks and Brain, vol. 2, pp. 991-996, October 13-15, 2005.

[16]   A.R. Sadeghian, J.D. Lavers, *Nonlinear Black-Box Modeling of Electric Arc Furnace: An Application of Fuzzy Logic Systems*: 1999 IEEE International Fuzzy Systems Conference Proceedings, vol.1, pp. 234-239, Seoul, Korea, August 22-25, 1999.

[17]   Y.F. Wang, J.G.Jiang, *A Novel Chaotic Model of AC Electric Arc Furnace for Power Quality Studies*: Proceeding of International Conference on Electrical Machines and Systems, pp. 1759-1762, Seoul, Korea, October 8-11, 2007.

[18]   Gregor Görtler, H. Peter Jörgl, *Energetically Optimized Control of an Electric Arc Furnace*: IEEE, International Conference on Control Applications, vol.1, pp.137-142, Taipei, Taiwan, September 2-4, 2004.

[19]   N. Köse, Ö. Salor, *New Spectral Decomposition Based Approach for Flicker Evaluation of Electric Arc Furnaces*: IET Generation, Transmission and Distribution, vol.3, issue 4, pp. 393-411, April 2009.

[20]   Güç Kalitesi Milli Projesi, http://www.guckalitesi.gen.tr, last visited on September 2009.

[21]   O. Salor, B. Gultekin, S. Burhan, et.al, *Electrical Power Quality of Iron and Steel Industry in Turkey*: Industry Applications Conference, 42nd IAS Annual Meeting, pp. 404-423, 2007.

[22]   M. Göl, Ö. Salor, B. Alboyacı, et.al, *A New Field-Data Based EAF Model for Power Quality Studies*: Industry Applications Conference, 43rd IAS Annual Meeting, pp. 1-11, Edmonton, Canada, October 2008

[23]   Enerji Piyasası Düzenleme Kurumu, *Elektrik İletim Sistemi Arz Güvenilirliği ve Kalitesi Yönetmeliği*: 10.11.2004.

[24]   IEEE Std. 519-1992, *IEEE Recommended Practices and Requirements for Harmonic Control in Electrical Power Systems.*

APPENDIX A

PARAMETERS OF THE EAF TRANSFORMER IN PLANT-1

TABLE A.1   EAF transformer ratings at Plant-1

Tap #	Power (kVA)	Voltage (V)	Current (A)	Voltage (V)	Current (A)	u_k (%)
18	90000		869.6	997.9	30062	10.14
15	90000		869.6	901.1	33292	13.09
10	73988	34500	714.9	740.8	33292	17.70
5	59263		572.6	593.4	33292	24.45
1	49938		482.5	520.5	33292	30.59

TABLE A.2   EAF series reactor ratings at Plant-1

Tap #	Voltage (V)	Power (kVAr)
11		32400
9	34500	25920
5		12960
1		0

TABLE A.3   EAF dip test measurement results at Plant-1

R_{SC21}	0.625 (mΩ)	X_{SC21}	2.459 (mΩ)	Z_{SC21}	2.537 (mΩ)
R_{SC22}	0.261 (mΩ)	X_{SC21}	2.904 (mΩ)	Z_{SC21}	2.916 (mΩ)
R_{SC23}	0.168 (mΩ)	X_{SC21}	2.558 (mΩ)	Z_{SC21}	2.564 (mΩ)
R_{SC2avg}	0.358 (mΩ)	X_{SC2avg}	2.640 (mΩ)	Z_{SC2avg}	2.672 (mΩ)

APPENDIX B

MATLAB CODE FOR THE VRL COMPUTATION

```matlab
load 'vi.mat'
[B,A]=butter(10,65/1600);

van=filter(B,A,va);
vbn=filter(B,A,vb);
vcn=filter(B,A,vc);
ian=filter(B,A,ia);
ibn=filter(B,A,ib);
icn=filter(B,A,ic);


[B,A] = BUTTER(10,40/1600,'high');

van=filter(B,A,van);
vbn=filter(B,A,vbn);
vcn=filter(B,A,vcn);
ian=filter(B,A,ian);
ibn=filter(B,A,ibn);
icn=filter(B,A,icn);

% determining zero cross

ima=1;
imb=1;
imc=1;

for n=1:1920000-1

    if (van(n,1)>0 || van(n,1)==0) && van(n+1,1)<0
        cyca(ima)=n;
        ima=ima+1;
    end

    if (vbn(n,1)>0 || vbn(n,1)==0) && vbn(n+1,1)<0
        cycb(imb)=n;
        imb=imb+1;
    end

    if (vcn(n,1)>0 || vcn(n,1)==0) && vcn(n+1,1)<0
        cycc(imc)=n;
        imc=imc+1;
    end
end
```

```matlab
for i=1:29998 % calculating impedance magnitude and phase angle

    VA=0;
    IA=0;
    a=0;
    b=0;
    VA=va(cyca(1,i):cyca(1,i+10),1); % 10 cycles sliding window
    IA=ia(cyca(1,i):cyca(1,i+10),1);

    a=fft(VA);
    b=fft(IA);

    varms=abs(a(11,1)/(length(VA)/2));
    varms=varms/sqrt(2);
    iarms=abs(b(11,1)/(length(IA)/2));
    iarms=iarms/sqrt(2);
    acia(i)=phase(a(11,1)/b(11,1));
    za(i)=varms/iarms;
    zaind(i)=round((cyca(1,i)+cyca(1,i+10))/2);

    VB=0;
    IB=0;
    a=0;
    b=0;

    VB=vb(cycb(1,i):cycb(1,i+10),1);
    IB=ib(cycb(1,i):cycb(1,i+10),1);

    a=fft(VB);
    b=fft(IB);

    vbrms=abs(a(11,1)/(length(VB)/2));
    vbrms=vbrms/sqrt(2);
    ibrms=abs(b(11,1)/(length(IB)/2));
    ibrms=ibrms/sqrt(2);
    acib(i)=phase(a(11,1)/b(11,1));
    zb(i)=vbrms/ibrms;
    zbind(i)=round((cycb(1,i)+cycb(1,i+10))/2);

    VC=0;
    IC=0;
    a=0;
    b=0;

    VC=vc(cycc(1,i):cycc(1,i+10),1);
    IC=ic(cycc(1,i):cycc(1,i+10),1);

    a=fft(VC);
    b=fft(IC);

    vcrms=abs(a(11,1)/(length(VC)/2));
    vcrms=vcrms/sqrt(2);
    icrms=abs(b(11,1)/(length(IC)/2));
    icrms=icrms/sqrt(2);
    acic(i)=phase(a(11,1)/b(11,1));
    zc(i)=vcrms/icrms;
    zcind(i)=round((cycc(1,i)+cycc(1,i+10))/2);
end
```

69

```matlab
% calculation of resistance and reactance

ra=za.*cos(acia);
rb=zb.*cos(acib);
rc=zc.*cos(acic);
xa=za.*sin(acia);
xb=zb.*sin(acib);
xc=zc.*sin(acic);

%determining the frequencies

ja=50;
jb=50;
jc=50;

for i=1:29997

    fa(i)=ja;
    ja=((zaind(i+1)-zaind(i))*312.5*10^-6)^-1;

    fb(i)=jb;
    jb=((zbind(i+1)-zbind(i))*312.5*10^-6)^-1;

    fc(i)=jc;
    jc=((zcind(i+1)-zcind(i))*312.5*10^-6)^-1;

end

fa (29998)=50;
fb (29998)=50;
fc (29998)=50;

%calculation of inductance values

la=(xa./(2*pi*fa));
lb=(xb./(2*pi*fb));
lc=(xc./(2*pi*fc));

%to avoid NaN values

zaind(1)=0;
zbind(1)=0;
zcind(1)=0;
zaind(29998)=1920000;
zbind(29998)=1920000;
zcind(29998)=1920000;

%interpolation

xi=1:1920000;
j=0;
rap=interp1(zaind,ra,xi);
rbp=interp1(zbind,rb,xi);
rcp=interp1(zcind,rc,xi);
lap=interp1(zaind,la,xi);
lbp=interp1(zbind,lb,xi);
lcp=interp1(zcind,lc,xi);
```

APPENDIX C

MATLAB CODE FOR THE HARMONIC CURRENT COMPUTATION

```matlab
aind=1;
bind=1;
cind=1;
han=[];
hbn=[];
hcn=[];
for n=0:29998

    a=ia(aind:cyca(n+10));
    b=ib(bind:cycb(n+10));
    c=ic(cind:cycc(n+10));
    af=fft(a);
    bf=fft(b);
    cf=fft(c);

    af(11)=0;
    af(length(af)-9)=0;
    bf(11)=0;
    bf(length(bf)-9)=0;
    cf(11)=0;
    cf(length(cf)-9)=0;

    afi=real(ifft(af));
    bfi=real(ifft(bf));
    cfi=real(ifft(cf));

    han(aind:cyca(n+1))= afi(1:cyca(n+1)-aind+1);
    hbn(bind:cycb(n+1))= bfi(1:cycb(n+1)-bind+1);
    hcn(cind:cycc(n+1))= cfi(1:cycc(n+1)-cind+1);

    a=0;
    af=0;
    b=0;
    bf=0;
    c=0;
    cf=0;
    aind=cyca(n+1)+1;
    bind=cycb(n+1)+1;
    cind=cycc(n+1)+1;
end
```

APPENDIX D

DETERMINATION OF THE HARMONIC CURRENT LIMITS

The maximum load current and the short circuit current of the power transformer are the main factors that determine the harmonic current limits. To find the maximum load current measurements as long as possible are conducted. The standard advises two-year-long measurements [24]. In this thesis work, seven-day measurements conducted by the National Power Quality Project are used. The maximum of the 15 minutes averages of the fundamental component (50 Hz) of the current is the maximum load current, I_k. The short circuit current, I_L, is specified by the power transformer between the iron and steel plant and the utility grid. The ratio of the I_L to I_k determines the limits for each harmonic current component. Table B.1 represents the allowed harmonic current limits for different I_L/I_k ratios.

TABLE D.1: Current Harmonic Limits Allowed in the Electricity Transmission System Supply Reliability and Quality Regulation

Harmonic Order		1<MV≤34.5 I_k/I_L					34.5<HV≤154 I_k/I_L					154<VHV I_k/I_L				
Group	No	<20	20-50	50-100	100-1000	>1000	<20	20-50	50-100	100-1000	>1000	<20	20-50	50-100	100-1000	>1000
O	3	4	7	10	12	15	2	3.5	5	6	7.5	1	1.8	2.5	3	3.8
D	5	4	7	10	12	15	2	3.5	5	6	7.5	1	1.8	2.5	3	3.8
D	7	4	7	10	12	15	2	3.5	5	6	7.5	1	1.8	2.5	3	3.8
	9	4	7	10	12	15	2	3.5	5	6	7.5	1	1.8	2.5	3	3.8
	11	2	3.5	4.5	5.5	7	1	1.8	2.3	2.8	3.5	0.5	0.9	1.2	1.4	1.8
	13	2	3.5	4.5	5.5	7	1	1.8	2.3	2.8	3.5	0.5	0.9	1.2	1.4	1.8
H	15	2	3.5	4.5	5.5	7	1	1.8	2.3	2.8	3.5	0.5	0.9	1.2	1.4	1.8
A	17	1.5	2.5	4	5	6	0.8	1.25	2	2.5	3	0.4	0.6	1	1.25	1.3
R	19	1.5	2.5	4	5	6	0.8	1.25	2	2.5	3	0.4	0.6	1	1.25	1.3
M	21	1.5	2.5	4	5	6	0.8	1.25	2	2.5	3	0.4	0.6	1	1.25	1.3
O	23	0.6	1	1.5	2	2.5	0.3	0.5	0.75	1	1.25	0.15	0.25	0.4	0.5	0.6
N	25	0.6	1	1.5	2	2.5	0.3	0.5	0.75	1	1.25	0.15	0.25	0.4	0.5	0.6
I	27	0.6	1	1.5	2	2.5	0.3	0.5	0.75	1	1.25	0.15	0.25	0.4	0.5	0.6
C	29	0.6	1	1.5	2	2.5	0.3	0.5	0.75	1	1.25	0.15	0.25	0.4	0.5	0.6
S	31	0.6	1	1.5	2	2.5	0.3	0.5	0.75	1	1.25	0.15	0.25	0.4	0.5	0.6
	33	0.6	1	1.5	2	2.5	0.3	0.5	0.75	1	1.25	0.15	0.25	0.4	0.5	0.6
	h>33	0.3	0.5	0.7	1	1.4	0.15	0.25	0.35	0.5	0.7	0.75	0.12	0.17	0.25	0.35

Even harmonics are limited with 0.25 times the limit of the next odd harmonic component.